1   Cellular, Circuit and Transcriptional Framework for Modulation of Itch in the Central

2   Amygdala

3   Vijay K Samineni[1], Jose G. Grajales-Reyes[1,2,3], Gary E Grajales-Reyes[5], Eric Tycksen[6],

4   Bryan A Copits[1], Christian Pedersen[4], Edem S Ankudey[1], Julian N Sackey[1], Sienna B

5   Sewell[1], Michael R Bruchas[1,7,8], and Robert W. Gereau IV[1,4,8]

6   [1]Washington University Pain Center and Department of Anesthesiology, [2]Medical

7   Scientist Training Program, [3]Neuroscience Program, [4]Department of Biomedical

8   Engineering, [5]Department of Pathology & Immunology, [6]Genome Technology Access

9   Center, Washington University School of Medicine; [7]Departments of Anesthesiology and

10   Pharmacology, University of Washington, Seattle, WA and [8]Departments of

11   Neuroscience and Biomedical Engineering, Washington University School of Medicine,

12   660 S. Euclid Ave, Box 8054, 63110 St. Louis, MO, USA

13   Lead Contact:

14   Robert W. Gereau IV

15   660 S. Euclid Ave.

16   Campus Box 8054

17   St. Louis, MO, 63110

18   gereaur@wustl.edu

19   Phone Number: 314-362-8312

20   Number of pages: 39

21   Number of figures: 6

22   Number of supplementary figures: 11

1

1 **Abstract**

2 Itch is an unpleasant sensation that elicits robust scratching and active avoidance.
3 However, the identity of the cells and neural circuits that organize this information remains
4 elusive. Here we show the necessity and sufficiency of itch-activated neurons in the
5 central amygdala (CeA) for both itch sensation and active avoidance. Further, we show
6 that itch-activated CeA neurons play important roles in itch-related comorbidities,
7 including anxiety-like behaviors, but not in some aversive and appetitive behaviors
8 previously ascribed to CeA neurons. RNA-sequencing of itch-activated CeA neurons
9 identified several differentially expressed genes as well as potential key signaling
10 pathways in regulating pruritis. Finally, viral tracing experiments demonstrate that these
11 neurons send a critical projection to the periaqueductal gray to mediate modulation of
12 itch. These findings reveal a cellular and circuit signature of CeA neurons orchestrating
13 behavioral and affective responses to pruritus in mice.

14

15

16

17

18

19

20

21

22

23

24

25

Main

As organisms have evolved, it has been essential that they acquire the means to sense physical and chemical threats in the world around them. One such threat detection system is itch, which accompanies unpleasant sensations that evoke strong urges to scratch and promote active avoidance behavior (Bautista et al., 2014; Han and Dong, 2014; Ikoma et al., 2006; LaMotte et al., 2014). Orchestrating adaptive behaviors (e.g. scratching an itch, avoidance of active threats) in the future requires rapid routing of information to brain regions that can encode memories and modify behavior based on prior experiences. The central amygdala (CeA) represents a strong candidate for these functions, as the CeA is thought to play a critical role in learning and modifying sensory and emotional memories and translating this information into apt adaptive behaviors (Fadok et al., 2018; Grundemann and Luthi, 2015; LeDoux and Daw, 2018). Recent studies have implicated the CeA in the regulation of itch (Albisetti et al., 2019; Chen et al., 2016; Ehling et al., 2018; Mu et al., 2017), and elevated activity in the CeA has been seen in patients during experimental itch (Papoiu et al., 2014; Vierow et al., 2015). Nevertheless, it is currently unknown how CeA neurons encode and modify the sensory or emotional components of itch. To address these questions, we used optical imaging, activity dependent labelling, neural tracing and cell activity-specific RNA sequencing to systematically investigate itch-activated CeA neurons and their projections in eliciting itch and its related comorbidities.

Results

To assess the potential activation of CeA neurons by itch in real time, we performed fiber photometry recordings to follow CeA neural activity during pruritogen-evoked scratching in awake, behaving mice. To record real-time Ca^{2+} dynamics in the CeA (Cui et al., 2013), we expressed the genetically-encoded calcium indicator, GCaMP6s, in CeA GABAergic neurons, using viral delivery of Cre-dependent GCaMP6s in Vgat-IRES-Cre mice (Swanson and Petrovich, 1998) (Fig. 1a and Supplementary Fig. 1a-c). Subcutaneous injection of chloroquine in the nape of the neck induced scratching behavior and resulted in robust increases in CeA neuronal activity (Fig. 1b). This activity commenced with initiation of scratching and stabilized whenever scratching stopped (Figure 1c-e), suggesting that the elevated activity was tightly-coupled with the act of scratching.
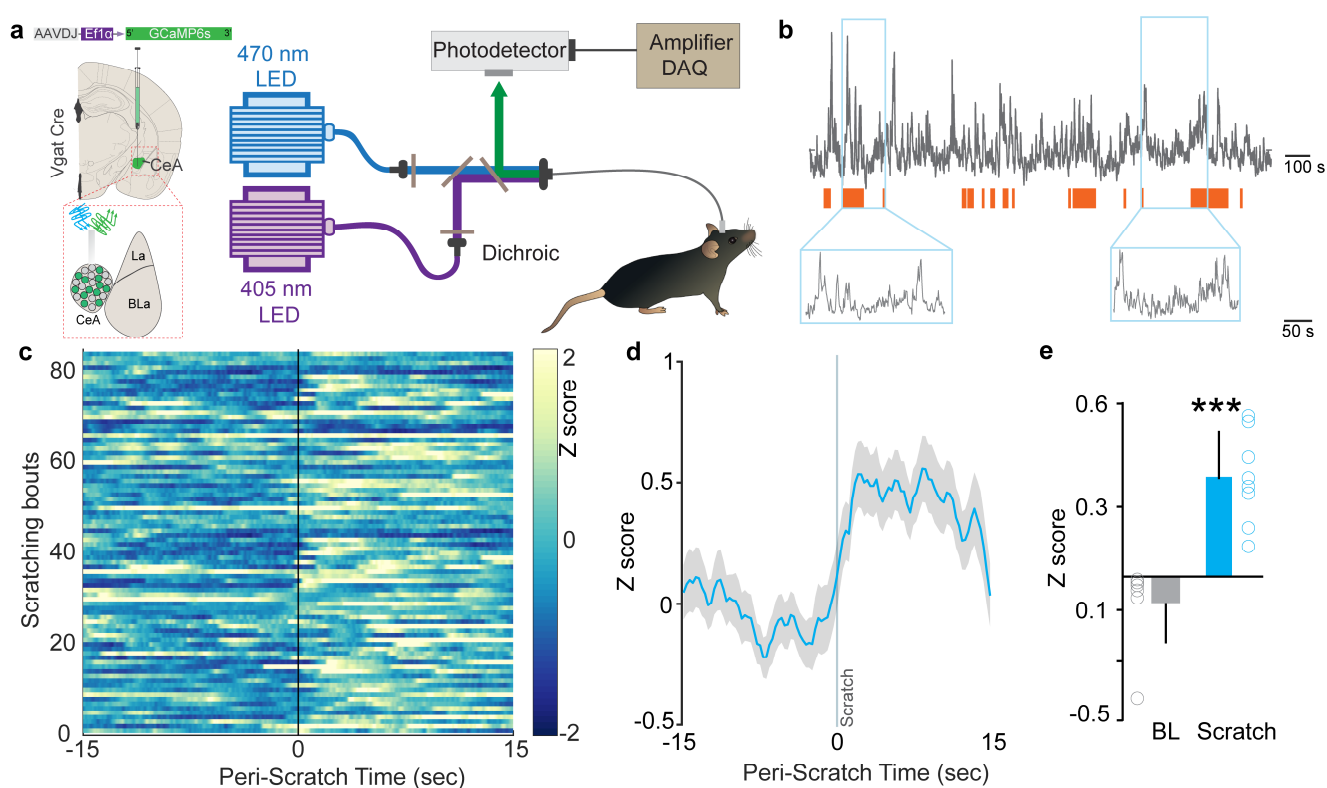

Fig 1. Neural dynamics of itch activated with CeA neurons. (a) Scheme demonstrating viral injection strategy and fiber placement to record CeAVgat neural activity in response to chloroquine. (b) Raw Ca2+ dynamics recorded from CeAVgat neurons and their relationship to chloroquine evoked scratching bouts (orange bars). (c) Heatmap showing Ca2+ dynamics of all trials of Vgat+ve vlPAG neurons relative to the initiation of chloroquine evoked scratching bouts (time zero). (d) Averaged GCaMP6s fluorescence signal of CeAVgat neurons showing rapid increases in fluorescence on the initiation of scratching bouts. Trace plotted as mean (blue line) ± SEM (gray shading), and the vertical line indicates initiation of scratching bouts. (e) Chloroquine-evoked scratching resulted in a significant increase in CeAVgat neuronal activity as measured by this change in GCaMP6s fluorescence. (N= 8, t test, t=5.923, df=14, P <0.0001).

1   Consistent with these real-time dynamic recordings, activity-dependent mapping studies

2   show robust cFos labelling bilaterally in the CeA following chloroquine injection in the

3   nape of the neck compared to saline-injected mice (Supplementary Fig. 1a, b). We

4   observed no significant differences in cFos labeling between right and left CeA

5   (Supplementary Fig. 1c).

6   These observations provide cellular confirmation of prior reports (Mochizuki et al.,

7   2014; Mochizuki et al., 2003; Papoiu et al., 2013) that indicated a possible role for the

8   CeA in itch processing, but the underlying neural circuitry remains to be identified. If CeA

9   neurons function as a key node in the circuit that tightly regulates sensory and affective

10   component of itch, then their activation should trigger potentiation of the itch-scratching

11   cycle and its aversive state. CeA neurons are molecularly heterogeneous and mediate

12   diverse behaviors generally related to negative affect (John et al., 2015; Kalin et al., 2004;

13   LeDoux, 2003; Ressler and Mayberg, 2007; Roozendaal et al., 2009; Tye et al., 2011),

14   so we reasoned global manipulation of CeA neuronal activity would not provide the

15   specificity needed to test the specific roles of itch-activated neurons. To enable the

16   desired selective manipulation of itch-specific neuronal populations in the CeA, we used

17   "Targeted Recombination in Active Populations" mice (Guenthner et al., 2013). These

18   mice express the tamoxifen-dependent CreER^{T2} recombinase from the *Fos* promoter.

19   CreER^{T2} expression is induced in neurons that were recently active. Catalytic activity of

20   CreER^{T2} is stabilized in the presence of 4-hydroxytamoxifen (4-OHT), resulting in

21   transgene recombination. By timing the administration of 4-OHT to coincide with recently

22   increased neuronal activity during acute chloroquine stimuli, we can gain permanent

23   genetic access to itch-responsive CeA neurons (aka FosTRAP mice). To test the validity

24   of this approach, we crossed FosTRAP mice to a Cre-dependent tdTomato flox-stop

25   reporter line (Madisen et al., 2010). We injected chloroquine or saline into the nape of the

26   neck, paired with injection of 4-hydroxytamoxifen (4-OHT) to induce Cre-mediated

27   recombination of the tdTomato in activated (cFos-expressing) neurons (Fig. 2a & b).

28   FosTRAPing with chloroquine treatment produced robust tdTomato expression in both

29   the right and left CeA (Fig. 2c, d & e), but not saline-treated controls (Supplementary Fig.

30   2e-g), consistent with our cFos staining results above. To confirm that the FosTRAPed

31   neurons are specific to the chloroquine-evoked scratching, one-week post-FosTRAP, we

5

immunostained for c-Fos protein in mice that received an additional chloroquine injection just prior to sacrificing (Fig. 2c & f). The majority of the tdTomato-positive CeA FosTRAPed neurons faithfully overlap with cFos-positive cells. These results demonstrate that we can efficiently gain genetic access to neurons that are activated by chloroquine.

To test whether reactivating itch-responsive CeA neurons can recapitulate itch behaviors, we expressed the Cre-dependent excitatory opsin, ChR2 (AAV5-EF1a-DIO-ChR2-eYFP) or a control virus (AAV5-EF1a-DIO-eYFP) in the right CeA of FosTRAP mice and FosTRAPed with chloroquine treatment as above (Fig. 2g). This produces expression of ChR2 specifically in CeA neurons responsive to itch, enabling their selective light-dependent activation. Optogenetic reactivation of FosTRAPed (ChR2$^+$) right CeA neurons resulted in significant spontaneous scratching and grooming behaviors compared to pre-stimulation baseline and photostimulation of eYFP-expressing control mice. Interestingly, although ChR2 was FosTRAPed by injecting chloroquine into the nape of the neck, we observed spontaneous scratching and grooming behaviors directed all over the body (data not shown) in a stimulation frequency-dependent manner (Fig. 2h, i). Even though some functions of the CeA are lateralized (Carrasquillo and Gereau, 2007), elicitation of itch behaviors are not lateralized to the right CeA as optical stimulation of FosTRAPed ChR2$^+$ neurons in the left CeA also resulted in significant spontaneous scratching behaviors compared to pre-stimulation baseline and photostimulation of eYFP-expressing controls (Supplementary Fig. 3). This result is consistent with the observation that chloroquine injection induces cFos expression in left and right CeA (Supplementary Fig. 2d). To further confirm these results and as a complementary approach, we expressed the Cre-dependent excitatory DREADD, hM3Dq (AAV5-hSyn-DIO-hM3Dq-mCh) or a control virus (AAV5-hSyn-DIO-mCh) in the CeA of FosTRAP mice. Chemogenetic activation of FosTRAPed CeA neurons also resulted in significant

1   spontaneous scratching behaviors (Supplementary Fig. 4e), consistent with the
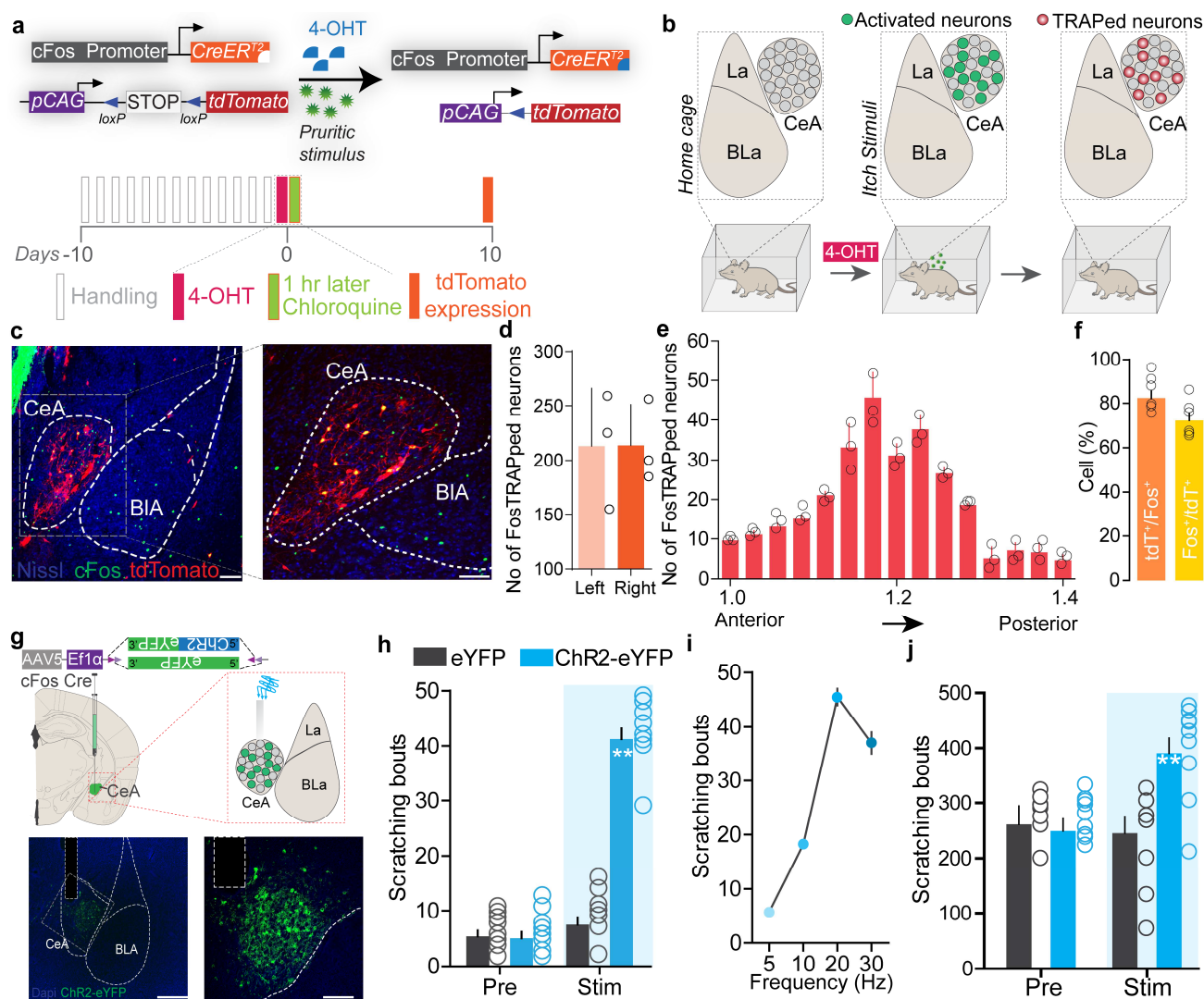
2   optogenetic results.

Fig 2. Itch-activated CeA neurons can drive pruritic behaviors. (a) FosTRAP strategy to selectively label itch-activated neurons in the CeA. (b) Scheme illustrating experimental strategy. (c) FosTRAPping with chloroquine-evoked scratching produces robust tdTomato expression in the CeA. Colocalization of itch-TRAPed neurons (red) in the CeA with cFos immunoreactivity (green) following a 2nd administration of chloroquine 7 days post. Scale bar = 85 and 250 µm. (d) Quantification of the number of FosTRAPped neurons in left and right CeA after chloroquine injection. n = 3 per group. t test, t=0.4339, df=2, p =0.70. (e) Rostro-caudal distribution of itch-TRAPed CeA neurons after chloroquine injection. (f) Colocalization of chloroquine-activated cFos with tdTomato+ve itch-TRAPed neurons. Relative percentages of Fos+ve neurons that are tdTomato+ve and tdTomato+ve neurons that are Fos+ve. n = 6 per group. t test, t=2.04 df=10, p =0.048. (g) Scheme to selectively express optogenetic constructs in itch-TRAPed CeA neurons. Illustration and representative section showing fiber optic placement above FosTRAPped CeA neurons expressing ChR2-eYFP (green). Scale bar, 100 µm. (h) Photostimulation (20 Hz) of itch-TRAPed CeA neurons produces robust spontaneous scratching. n = 6–11 per group. Pre Vs. Stim, F (1,30) = 3; eYFP Vs. ChR2, F (1,14) = 3.24, p = 0.0001. (i) Increases in scratching are frequency dependent. n = 6 per group. (j) Optical activation of itch-TRAPed CeA neurons potentiates chloroquine-evoked scratching while no changes were observed in control mice. n = 7 per group. Pre Vs. Stim, F (1,12) = 33.15; BL Vs. Stim in ChR2, F (1, 6) = 6.915, p = P=0.0391.

7

In contrast, stimulation of FosTRAPed neurons has no significant effect on hindpaw thermal sensitivity (Supplementary Fig. 5b) or licking and biting behaviors Supplementary Fig. 4f). However, stimulation of FosTRAPed neurons slightly increased mechanical sensitivity suggesting that these neurons can encode generalized itch-related behavior and hypersensitivity to mechanical stimuli (Supplementary Fig. 5c). These results suggest that FosTRAPed neurons might be involved in nociceptive processing (Neugebauer and Li, 2002). To further determine how reactivation of itch-activated (ChR2$^+$) FosTRAPed neurons (hereafter referred to as "itch-TRAPed neurons") can affect ongoing itch behaviors, we administered chloroquine and optically activated itch-TRAPed CeA neurons. Chloroquine evoked scratching was potentiated with optical reactivation of CeA itch-TRAPed neurons while no changes were observed in the eYFP controls (Fig. 2j). Chemogenetic stimulation of itch-TRAPed neurons produced similar results (Supplementary Fig. 4h).

Itch is an aversive sensory experience in humans and rodents (Desbordes et al., 2015; Mochizuki et al., 2015; Mochizuki et al., 2014; Papoiu et al., 2012; Papoiu et al., 2013), and the CeA mediates aversive phenotypes (Carrasquillo and Gereau, 2007; Ciocchi et al., 2010; Ehrlich et al., 2009; Haubensak et al., 2010; Tovote et al., 2016). Therefore, we wanted to assess whether itch-TRAPed CeA neurons encode negative valence associated with itch. We performed closed-loop real-time place-testing (RTPT) to assess affective state, where an animal freely explores two chambers but receives photostimulation of ChR2^{+ve} itch-TRAPed neurons in only one chamber. Reactivation of itch-TRAPed neurons produced robust place aversion to the stimulated side of the chamber while eYFP-FosTRAPed controls did not (Fig. 3b-d), thus demonstrating that itch-activated CeA neurons carry negative reinforcement signals.

Patients with pruritic skin disorders exhibit heightened anxiety (Ginsburg, 1995) and prior studies have shown CeA as a critical hub in coordinating anxiety states (Ahrens et al., 2018; Shackman and Fox, 2016). Therefore, we evaluated if reactivation of itch-TRAPed CeA neurons can drive anxiety-like behavior using the elevated zero maze (EZM) assay and open-field test (OFT). Optogenetic and chemogenetic reactivation of itch-TRAPed neurons lead to a profound decrease in time spent in the open arms of EZM
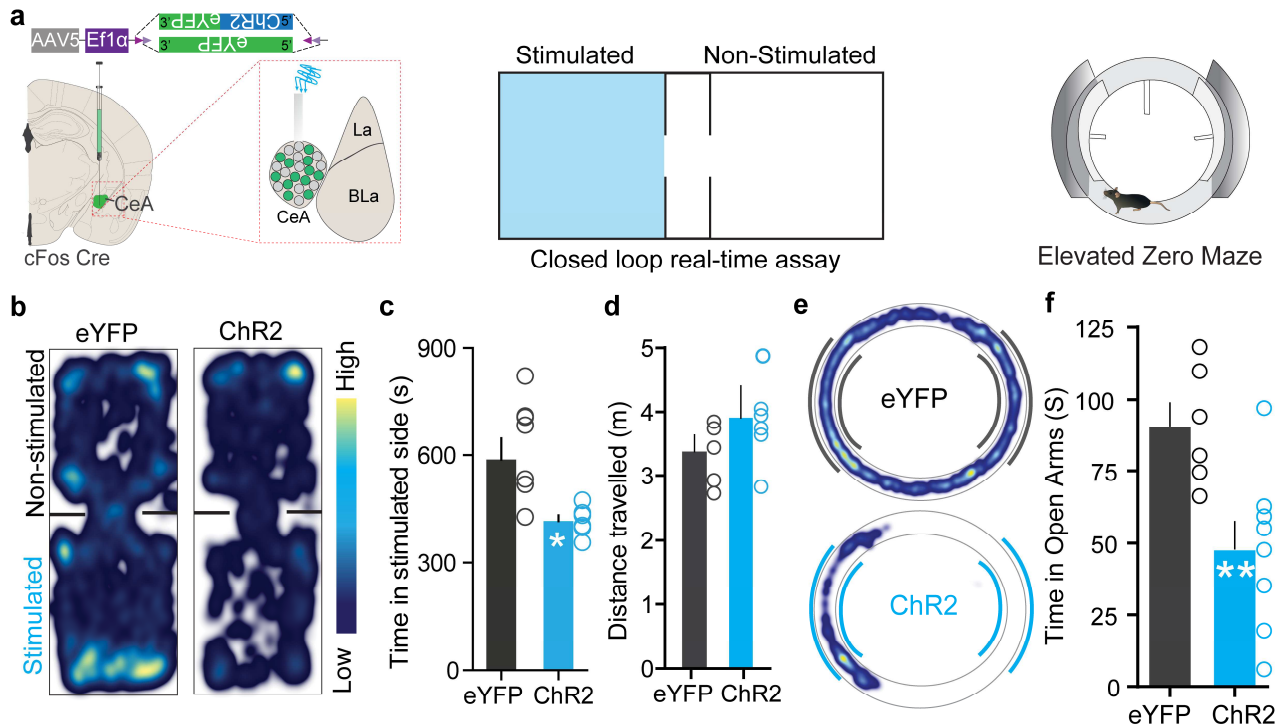
Fig. 3 Itch-activated CeA neurons are negatively reinforcing. (a) Illustration of strategy to express ChR2/eYFP selectively in itch-TRAPed neurons of the CeA. Experimental schematic of closed loop real-time assay and elevated zero maze. (b) Real-time place aversion assay with spatial location heatmaps of ChR2 and eYFP mice during closed loop optical stimulation. t test, t=2.806, df=12, p =0.0159. (c) Total time spent and (d) distance travelled in the photostimulation-paired chamber for ChR2 and eYFP mice. n = 7 per group, t test, t=0.7510, df=12, p =0.4142. (e) Representative occupancy heat map showing spatial location in the elevated zero maze (EZM)of a control mouse (eYFP) and a mouse injected with DIO-ChR2. (f) Optogenetic activation of itch-TRAPed CeA neurons causes a significant reduction in time spent in open arms in EZM. Light stimulation was delivered entire time mice were on EZM n= 6-10 per group. t test, t=5.922, df=12, p =0.0086.

1 compared to controls, indicating anxiogenic-like behavioral state (Fig. 3e-,

2 Supplementary Fig. 6b, c). Reactivation of these neurons also lead to decreased time

3 spent in the center during the OFT, further suggesting these neurons can drive anxiety-

4 like behavior (Supplementary Fig. 6d-i). Notably, opto- and chemogenetic reactivation of

5 FosTRAPed neurons did not drive freezing or flight responses in open-field test

6 (Supplementary Fig. 6e & g), suggesting these neurons are not involved in fear-like

7 behaviors. Furthermore, stimulation of these neurons also had no effect on feeding and

8 other appetitive behaviors the CeA is reported to evoke (Douglass et al., 2017; Han et al.,

9 2017; Kim et al., 2017; Li et al., 2013 (Supplementary Fig. 7a-c & Supplementary Fig. 8).

10 Having shown that itch-TRAPed CeA neurons are sufficient to drive itch-related

11 sensory and affective behaviors, we aimed to determine if endogenous activity of these

12 neurons is necessary for itch-related behaviors. We selectively inhibited itch-responsive

9

1   CeA neurons by expressing the Cre-dependent inhibitory DREADD, hM4Di (AAV5-hSyn-

2   DIO-hM4Di-mCh), or a control virus (AAV5-hSyn-DIO-mCh) in itch-activated CeA

3   neurons of FosTRAP mice (Fig. 4a-c). CNO application to ex vivo CeA slices from itch-

4   TRAPed mice decreased neuronal excitability to suprathreshold stimuli (Fig. 4d).

5   Chemogenetic inhibition of CeA itch-TRAPed neurons by CNO injection significantly

6   attenuated chloroquine-evoked scratching compared to pre-CNO baseline and compared

7   to mCherry-expressing controls (Fig. 4e, f). These results suggest that itch-activated (itch-

8   TRAPed) CeA neurons are necessary for chloroquine induced scratching behavior. We

9   observed no significant effect on thermal or mechanical sensitivity by inhibiting CeA itch-

10   TRAPed neurons (Supplementary Fig. 5d, e). Furthermore, silencing CeA itch-TRAPed

11   neurons did not lead to freezing or flight responses or anxiolytic effects (Supplementary
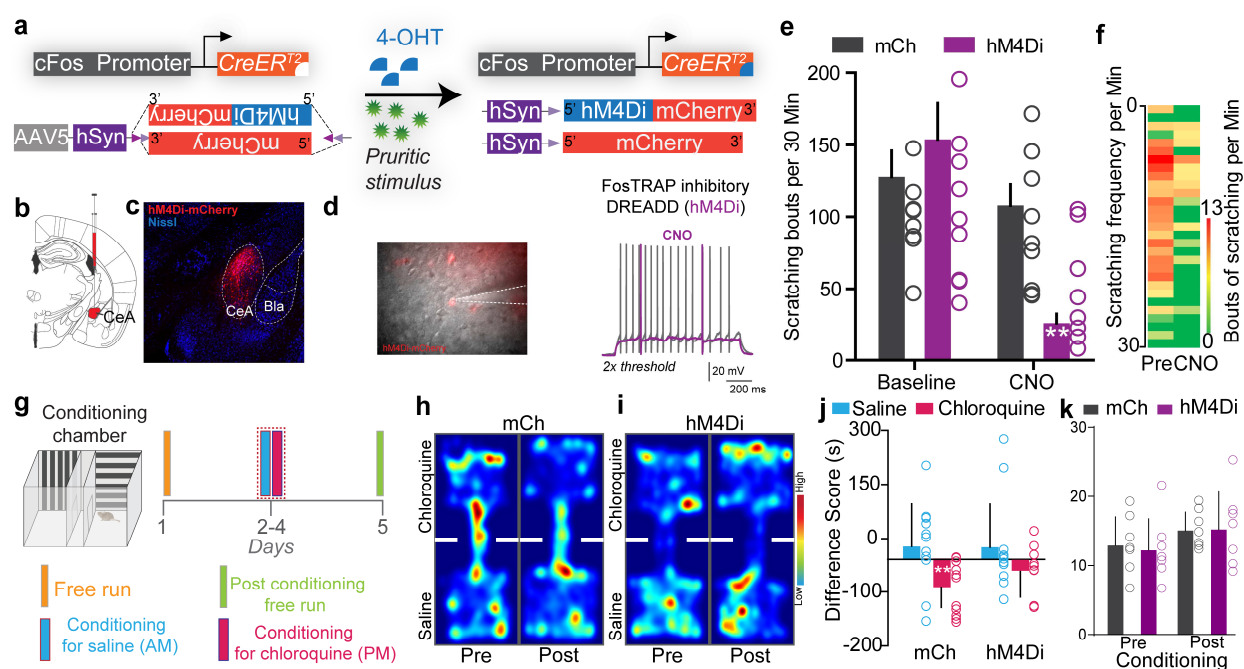

Fig 4. Inhibiting itch-activated CeA neurons impairs aversive learning associated with itch. (a) Illustration of strategy to express inhibitory DREADDs selectively in itch-TRAPed neurons of the CeA. (b) Experimental timeline to FosTRAP DREADDs in CeA neurons. (c) Representative section showing itch-TRAPed CeA neurons expressing hM4Di-mCherry (Red). Scale bar, 75 μm. (d) Infrared DIC image of CeA itch-TRAPed neurons expressing hM4Di-mCherry. In hM4Di+ve CeA neurons, CNO bath application decreased neuronal excitability to suprathreshold stimuli. (e) Chemogenetic inhibition of itch-TRAPed CeA neurons leads to a significant reduction in chloroquine evoked scratching. CNO has no effect on chloroquine-evoked scratching in control mice expressing mCherry. n = 8–9 per group. p = 0.0011. (f) Heat map showing averaged chloroquine-evoked scratching bouts pre- and post-CNO in mice expressing hM4Di in CeA. (g) Schematic and timeline of conditioned place aversion experimental design with chemogenetic silencing. Representative heat map showing spatial location of a control mouse injected with the DIO-mCh (h) and the DIO-hM4Di DREADD virus (i), pre- and post-chloroquine conditioning. (j) Change in chamber occupancy time in the chloroquine-paired chamber compared to the saline-paired chamber after chemogenetic silencing. n = 11 per group. p = 0.044. (K) Distance travelled in chloroquine paired chamber did not differ pre- and post-conditioning in mCh and hM4Di mice. n = 0.769 per group.

1   Fig. 6j-n). Inhibition of itch-TRAPed neurons also did not affect feeding (Supplementary

2   Fig. 7d) and appetitive behaviors (Supplementary Fig. 8). Because activating CeA itch-

3   TRAPed neurons lead to robust avoidance, we hypothesized that inhibiting these neurons

4   would block conditioned place aversion (CPA) to chloroquine. We performed CPA to

5   chloroquine in itch-TRAPed mice expressing either hM4Di or mCherry in itch-responsive

6   neurons (Fig. 4g). Silencing itch-TRAPed (hM4Di[+ve]) CeA neurons with CNO injection in

7   the chloroquine-paired chamber during conditioning blocked CPA to chloroquine, while

8   CNO-treated mCherry controls exhibited CPA to chloroquine, suggesting that these

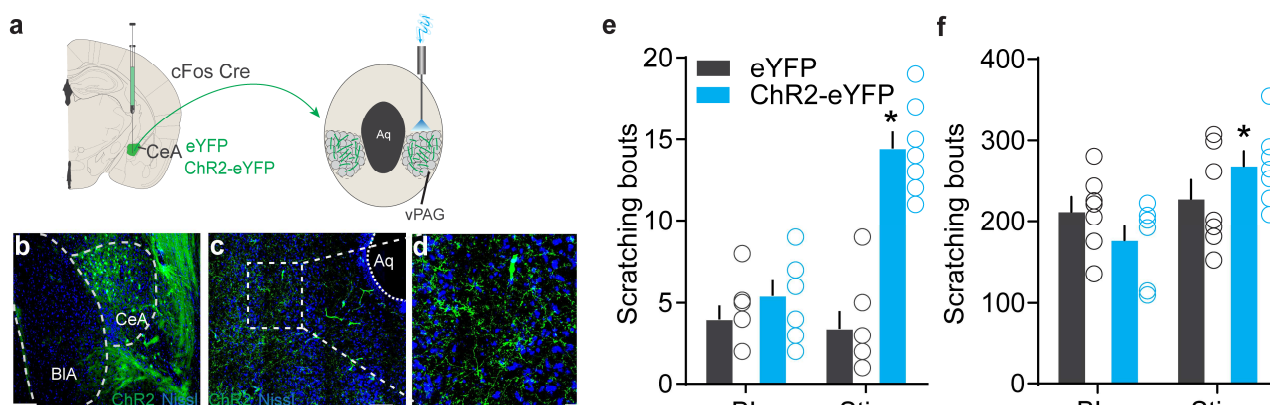9   neurons can robustly modulate the aversive component of itch (Fig. 4h-k).

Fig 5. Identification of the downstream circuit of itch-activated CeA neurons. (a) Scheme showing expression of ChR2 in itch-TRAPed CeA neurons and their axonal photostimulation in the vPAG. (b) FosTRAPped CeA neurons expressing ChR2-eYFP. Scale bar, 125 μm. (c, d) Itch-TRAPed ChR2+ve CeA axonal terminals ramify densely in the vPAG. Scale bar, 100 and 25 μm. (e) Optogenetic stimulation of FosTRAPed ChR2+ve axonal projections from CeA in the vPAG resulted in significant spontaneous scratching, whereas photostimulation had no effect on scratching in control mice. Pre vs Stim, F (1,12) = 33.15, p <0.0001, n = 5-7 per group. (f) Optical activation of itch-TRAPed CeA neurons potentiates chloroquine-evoked scratching while no changes were observed in control mice. n = 7 per group. BL Vs. Stim in eYFP, F (1,6) = 0.019, P=0.8924; BL Vs. Stim in ChR2, F (1, 6) = 9.109, P=0.0235.

10   We next sought to understand the circuit context of these itch-activated CeA

11   neurons and explored the downstream nodes that might mediate expression of scratching

12   behaviors. We found that itch-TRAPed CeA neurons send notably dense axonal

13   projections in the ventral periaqueductal gray (vPAG) (Fig. 5a-d). We confirmed these

14   results by injection CTB into the vPAG (Supplementary Fig. 9a, b) and also by injecting

15   retro Cre DIO GFP in to the vPAG in Vgat cre mice (Supplementary Fig. 9c, d). Injection

16   of RV-GFP into vlPAG of Vgat and Vglut2 Cre mice labeled monosynaptic projections

17   from the CeA consistent with prior work (Supplementary Fig. 9e-k). Because the vPAG

18   has previously been shown to contribute to pruritic behaviors (Gao et al., 2019; Samineni

11

1   et al., 2019), we focused our functional studies on this CeA→vPAG circuit. If this

2   CeA→vPAG circuit mediates scratching behaviors elicited by the itch-TRAPed CeA

3   neurons, then stimulating this projection should recapitulate these behaviors. As

4   predicted, photostimulating ChR2-expressing itch-TRAPed CeA neuronal terminals in the

5   vPAG recapitulated spontaneous scratching behaviors (Fig. 5e). Activating itch-TRAPed

6   CeA neuronal terminals in the vPAG did not produce freezing or flight responses. To

7   determine if reactivation of itch-TRAPed CeA→vPAG projections (ChR2$^+$) can influence

8   ongoing itch behaviors, we administered chloroquine and optically activated itch-TRAPed

9   CeA→vPAG projections. Chloroquine evoked scratching was potentiated with optical

10 reactivation of CeA→vPAG projections while no changes were observed in the eYFP

11 controls (Fig. 5f). These results show that the CeA→vPAG neuronal circuit is crucial node

12 in mediating pruritic behaviors.

13   Lastly, we performed RNA-seq to identify transcriptional profiles of itch-activated

14 CeA cells (Fig. 6a). To do this, we TRAPed tdTomato in itch-activated CeA neurons as

15 described above, and separated the itch-TRAPed neurons from adjacent tdTomato^{-ve}

16 cells for comparative RNA-seq analysis. Correlation analysis of RNA-seq data revealed

17 itch-TRAPed tdTomato^{+ve} cells and TRAPed tdTomato^{-ve} cells are clustered apart from

18 each other (Supplementary Fig. 11c). In our sequencing results, we observed that both

19 the tdTomato^{+ve} and tdTomato^{-ve} cells expressed Slc32A1 transcript (VGAT, a marker for

20 GABAergic neurons), consistent with the notion that the majority of CeA neurons are

21 GABAergic. Hierarchical clustering analysis of genes shows highly correlated gene

22 expression patterns that show unique expression profiles in FosTRAPed^{+ve} CeA neurons

23 vs FosTRAPed^{-ve} CeA neurons (Supplementary Fig. 11d). We identified numerous highly

24 correlated gene clusters based on their expression levels in FosTRAPed^{+ve} neurons

25 (Supplementary Fig. 11e). Subsequent analysis of itch-TRAPed neurons revealed

26 significant enrichment of several unique transcripts in the itch-activated neurons (Fig. 6b).

27 Weighted gene correlation network analysis (WGCNA) of genes identified a cluster of up-

28 regulated genes 99% correlated and highly significant for itch-activated neurons

29 (Supplementary Fig. 11f-h). To link transcriptional profiles of FosTRAPed cells to known

30 CeA functional pathways, we performed pathway analysis. From KEGG and Gene Set

31 Enrichment Analysis (GSEA), we have identified changes in the expression of functionally
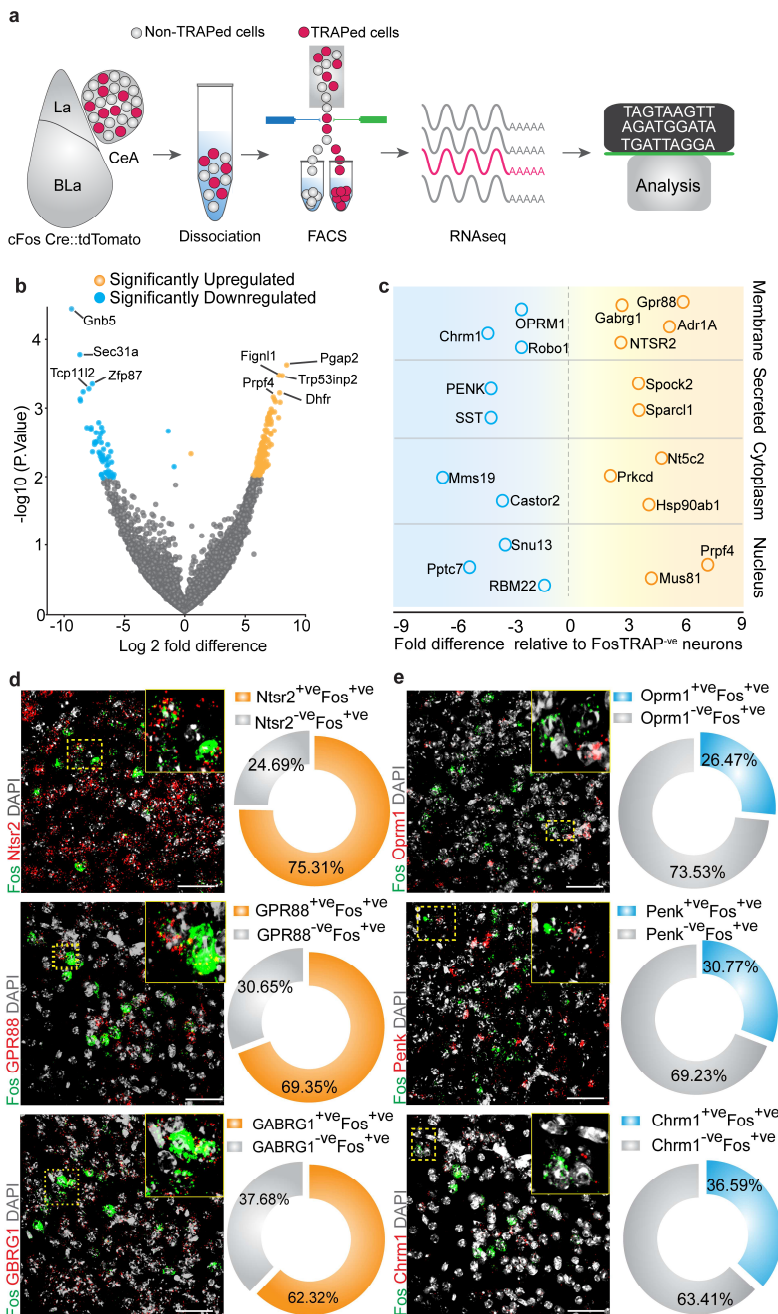
Fig 6. Cell-type specific transcriptomic profiling of itch-activated CeA cells. (a) Experimental workflow outlining fluorescence-activated-cell-sorting (FACS) of the FosTRAPped tdTomato+ve and tdTomato-ve CeA neurons for whole-cell transcriptomics analyses. (b) Volcano plot of Log2-fold change (x axis) and p values (y axis) showing the transcripts that are differentially expressed in the itch-TRAPed tdTomato+ve CeA cells. Significantly differentially expressed genes are color coded and genes that have P <= 0.001 are indicated on the plot. (c) Candidate genes identified by fold change in expression of genes in significantly enriched KEGG pathways from the FosTRAPped tdTomato+ve CeA cells. (d) Multiplexed FISH was used in validating the expression of NTSR2, GPR88 and GABARG1 in itch activated Fos+ve CeA cells. We observed considerable overlap between NTSR2+ve (75.31% cells), GPR88+ve (69.35%) and Gabrg1+ve (62.32% cells) with itch activated Fos+ve cells in the CeA. (e) Multiplexed FISH was used to verify the overlap of OPRM1, Penk and Chrm1 in itch activated Fos+ve CeA cells. We find their partial overlap of Fos+ve cells in the CeA with cells that express OPRM1+ve (26.47% cells) Penk+ve (30.77% cells) and Chrm1+ve (36.50% cells). Right corner of each image shows magnification of the inset (yellow box).

related candidate genes that are enriched in several pathways (Fig. 6c). We have identified significantly enriched CeA candidate genes that might be associated with pruritus regulation, as well as significantly genes expressed at significantly lower levels relative to the non-TRAPped cells that could be involved in the suppression of pruritus. To independently confirm our RNAseq findings, we performed dual-color fluorescent in situ hybridization (FISH) to visualize mRNA expression of several candidate genes enriched specifically only in the fos-positive cells induced by pruritic stimuli. We observed considerable overlap between NTSR2[+ve] (75.31% cells per 4 sections), GPR88[+ve] (69.35% cells per 4 sections) and Gabrg1[+ve] (62.32% cells per 4 sections) cells with itch activated Fos[+ve] cells in the CeA (Fig. 6d), which were shown to be significant enriched in itch-TRAPed tdTomato[+ve] cells. To

13

1 confirm whether this overlap is specific only to the enriched gene cluster, we also
2 assessed the overlap between itch activated Fos^{+ve} cells in the CeA and cluster of genes
3 with significantly lower expression in the itch-TRAPed neurons observed from RNAseq
4 data. We find their partial overlap of Fos^{+ve} cells in the CeA (Fig. 6e) with cells that express
5 OPRM1^{+ve} (26.47% cells per 4 sections) Penk^{+ve} (30.77% cells per 4 sections) and
6 Chrm1^{+ve} (36.50% cells per 4 sections). These results confirm our findings of differentially
7 expressed genes in itch-activated CeA cells and suggesting that further mining of these
8 sequencing data by the community will reveal important new findings related to itch and
9 its comorbidities.

10 **Discussion**

11 While there is robust evidence demonstrating the role spinal cord circuits play in
12 driving itch behaviors (Bautista et al., 2014; Han and Dong, 2014; LaMotte et al., 2014;
13 Ross et al., 2010; Sun et al., 2009), the identity and properties of neural circuits in the
14 brain that coordinate pruritic behaviors are still poorly understood. Neural circuits in the
15 central amygdala are implicated in pruritic process (Chen et al., 2016; Mu et al., 2017),
16 but cells and circuits that can alter pruritic processing in the CeA has been unclear. The
17 CeA is well known to regulate a wide variety of aversive (Carrasquillo and Gereau, 2007;
18 Ciocchi et al., 2010; Crock et al., 2012; Ehrlich et al., 2009; Haubensak et al., 2010;
19 Tovote et al., 2016) and appetitive behaviors (Cai et al., 2014; Carter et al., 2013;
20 Douglass et al., 2017; Hardaway et al., 2019; Kim et al., 2017; Robinson et al., 2014;
21 Warlow et al., 2020). Here, we propose a cellular and circuit framework of the CeA in
22 pruritis and its associated affect modulation. By gaining genetic access to neurons that
23 are active specifically during itch, we were able to selectively identify a diverse repertoire
24 of sensory and aversive behavioral responses mediated by itch-responsive CeA neurons.
25 Activation of itch-responsive neurons in right or left CeA is sufficient to recapitulate
26 spontaneous itch behaviors, potentiate chloroquine-evoked itch and produce aversive
27 and anxiety-related behaviors. Furthermore, inhibiting these neurons is sufficient to
28 attenuate ongoing itch and block its associated aversive component. Our findings reveal
29 the presence of an itch-responsive neuronal population in the CeA that is necessary and
30 sufficient to drive itch-related sensory and affective behaviors. We used both optogenetics

14

1 and chemogenetics in a complementary manner to confirm these results. Conceptually,

2 our findings seem to reconcile prior work (Chen et al., 2016; Mochizuki et al., 2020;

3 Papoiu et al., 2014; Sun et al., 2009; Vierow et al., 2015) suggesting a pivotal role of CeA

4 neurons in pruritic processing. The CeA is known to be involved in threat detection, and

5 to produce adaptive responses when organisms encounter threatening conditions (Fadok

6 et al., 2018; Grundemann and Luthi, 2015; LeDoux and Daw, 2018). These itch

7 responsive CeA neurons could be a gateway in controlling itch and its associated affective

8 component.

9   Activation of itch-TRAPed CeA neurons elicits aversive behaviors like place

10 aversion and anxiety like behaviors, while inhibition of itch-TRAPed CeA neurons

11 produces robust blockade of place aversion to chloroquine. It is well established that the

12 CeA mediates stress induced anxiety behaviors (Botta et al., 2015; Kalin et al., 2004; Li

13 et al., 2017; Weera et al., 2020), but our results show that silencing itch-TRAPed CeA

14 neurons does not have any effect on basal anxiety like behavior. Future experiments

15 should address whether these neurons are capable of attenuating anxiety during a variety

16 of threats or stressors. Our findings also imply that itch-activated CeA neurons may also

17 be involved to some extent in regulating nociceptive transmission. Itch-activated CeA

18 neurons that drive pruritic processing could represent a subset or overlapping populations

19 that also process nociceptive information. Our additional experiments also suggest that

20 the CeA itch responsive neurons do not have any effect on feeding, reward seeking, motor

21 and freezing behaviors. It is possible these behaviors are driven by distinct molecularly

22 defined cell types in the CeA (Cai et al., 2014; Carter et al., 2013; Ciocchi et al., 2010;

23 Douglass et al., 2017; Ehrlich et al., 2009; Hardaway et al., 2019; Haubensak et al., 2010;

24 Kim et al., 2017; Robinson et al., 2014; Tovote et al., 2016; Warlow et al., 2020) that are

25 distinct from the itch-activated CeA neurons we have studied here.

26   We found that itch-activated CeA neurons send functional outputs to the vPAG,

27 and activating these CeA→vPAG projections is sufficient to drive scratching. These

28 findings are consistent with recent reports (Gao et al., 2019; Samineni et al., 2019)

29 showing that activating PAG^{Vglut2} and PAG^{Tac1} neurons produces robust scratching in

30 mice. Based on the results from the present study and reconciling with prior work, a

15

1　reasonable hypothesis is that information from itch-activated CeA neurons promotes

2　scratching via disinhibition of the PAG^{Tac1} output neurons. As activating these PAG

3　populations does not elicit freezing or escape behaviors, it is possible that PAG neurons

4　that process pruritic information may be distinct from the ones that drive freezing, escape

5　or nociceptive behaviors. Based on our findings, pruritic information arriving in PAG

6　neurons originates at least in part via a CeA itch responsive neuronal population, and

7　contributes to the processing and generation of adaptive responses to pruritis. Our

8　RNAseq data show that CeA neurons are GABAergic, and anatomical tracing data

9　indicate that CeA neurons that project to the PAG are GABAergic inhibitory populations

10　(Supplementary Fig. 9d). Recent work shows that CeA GABAergic neurons that project

11　to vlPAG can elicit freezing, escape (Haubensak et al., 2010; Tovote et al., 2016), hunting

12　(Han et al., 2017), sleep (Snow et al., 2017) and nociception (Avegno et al., 2018; Li and

13　Sheets, 2018; Yin et al., 2020). In our work, we found that the itch-activated CeA→PAG

14　projections drive pruritic behaviors without evoking freezing or escape behaviors,

15　suggesting that these FosTRAPed CeA→PAG projections are distinctly tuned to elicit

16　scratching. The cellular and molecular identities that distinguish these projections from

17　other CeA neurons is yet to be identified (Steinberg et al., 2020). A critical task in the

18　future will be to identify and characterize how these different modalities of information are

19　differentially processed via these projections and how the postsynaptic neurons in the

20　PAG differentiate this information to transform it into behavioral output. Here we establish

21　a critical role for inhibitory projections from CeA to PAG in pruritic regulation. Further

22　studies will be required to more fully understand the mechanisms by which this projection

23　drives itch and associated affective behaviors.

24　The CeA is highly molecularly heterogeneous region that is known to express a diverse

25　array of neuropeptides, receptors and cellular machinery that are unique to CeA in

26　integrating and orchestrating neuromodulatory functions (Kim et al., 2017; Zirlinger and

27　Anderson, 2003; Zirlinger et al., 2001). To understand the unique genetic identity of CeA

28　neurons that regulate pruritic behaviors, we performed RNAseq of itch-activated CeA

29　neurons by TRAPing these neurons with pruritic stimuli. These activity-dependent RNA-

30　Seq data show extensive molecular programs that are selectively enriched in the itch

31　responsive neurons relative to other cells in CeA.   We observe significant enrichment of

1   NTSR2, GPR88 and Gabrg1 in itch-activated neurons, and relatively lower expression of

2   OPRM1, PENK and Chrm1, suggesting that these genes could be critical candidates in

3   regulating pruritis and its associated anxiety. In our analysis we have followed up on 6

4   candidate genes, but the dataset we have generated here will be an immensely valuable

5   resource to the neuroscience community interested in the role of CeA neurons in

6   modulation of sensory and affective behaviors.

7   **Methods**

8   **Animals** All experiments were conducted in accordance with the National Institute of

9   Health guidelines and with approval from the Animal Care and Use Committee of

10   Washington University School of Medicine. Mice were housed on a 12-hour light-dark

11   cycle (6:00am to 6:00pm) and were allowed free access to food and water. All animals

12   were bred onto C57BL/6J background and no more than 5 animals were housed per

13   cage. Male littermates between 8-12 weeks old were used for experiments. *FosCreERT2*

14   *mice (B6.129(Cg)-Fostm1.1(cre/ERT2)Luo/J; stock #21882, Ai9-tdTomato mice (B6.Cg-*

15   *Gt(ROSA)26Sortm9(CAG-tdTomato)Hze/J; stock #007909,* Vgat-ires-Cre

16   (*Slc32a1^{tm2Lowl}; stock #028862.*), Vglut2-ires-Cre (*Slc17a6^{tm2Lowl};* stock # 028863$^{.}$) and

17   C57BL\6J mice were purchased from Jackson Laboratories and colonies were

18   established in our facilities. For all the behavioral experiments heterozygous cFos-Cre

19   male mice were used, for Cfos co-staining and sequencing experiments were performed

20   on heterozygous cFos-Cre male mice crossed to homozygous Ai9mice from Jackson

21   Laboratory. Litters and animals were randomized at the time of assigning experimental

22   conditions for the whole study. Experimenters were blind to treatment and genotype.

23   **Viral constructs** Purified and concentrated adeno-associated viruses coding for Cre-

24   dependent hM3Dq-mCherry(rAAV5/hSyn-DIO-hM3Dq-mCherry; 6 x 10^{12} particles/ml, Lot

25   number: AV4495c and Lot date: 02/23/2012) and hM4D-mCherry (rAAV5/hSyn-DIO-

26   hM4Di-mCherry; 6 x 10^{12} particles/ml, Lot number: AV4496c and Lot date: 11/20/2012),

27   control mCherry (rAAV5/hSyn-DIO-mCherry; 3.4 x 10^{12} particles/ml, Lot number: AV5360

28   and Lot date: 04/09/2015), ChR2- eYFP (rAAV5-DIO-ChR2-eYFP; 4.8 x 10^{12} particles/ml,

29   Lot number: AV4313Y and Lot date: 04/21/2017) and control eYFP (rAAV5-DIO-eYFP;

30   3.3 x 10^{12} particles/ml, Lot number: AV4310i and Lot date: 07/21/2016) was used to

express in the FosCreERT2 mice. Helper virus, AAV1-EF1α-FLEX-TVAmCherry (rAAV5/ EF1α-FLEX-TVAmCherry; 4 x 10^{12} particles/ml) and AAV1-CAG-FLEX-RG (rAAV5/ CAG-FLEX-RG; 3 x 10^{12} particles/ml) were mixed at a ratio of 1:3 and then injected into the vPAG. Three weeks later, EnvA G-deleted Rabies-GFP (3.9 x 10^9 particles/ml) was injected in the vPAG. All vectors except Rabies virus were packaged by the University of North Carolina Vector Core Facility. Rabies virus was purchased from Salk Gene Transfer, Targeting and Therapeutics Core. All vectors were aliquoted and stored in -80°C until use.

Stereotaxic Surgeries Mice were anesthetized with 1.5 to 2.0% isoflurane in an induction chamber using isoflurane/breathing air mix. Once deeply anesthetized, mice were secured in a stereotactic frame (David Kopf Instruments, Tujunga, CA) where surgical anesthesia was maintained using 2% isoflurane. Mice were kept on a heating pad for the duration of the procedure. Preoperative care included application of sterile eye ointment for lubrication, administration of 1mL of subcutaneous saline and surgery site sterilization with iodine solution. A small midline dorsal incision was performed to expose the skull and viral injections were performed using the following coordinates: CeA, -1.24 mm from bregma, +/- 2.8 mm lateral from midline and 4.5 mm ventral to skull. Viruses were delivered using a stereotaxic mounted syringe pump (Micro4 Microsyringe Pump Controller from World Precision Instruments) and a 2.0uL Hamilton syringe. Injections of 75-100 nL of the desired viral vectors into the area of interest were performed at a rate of 1uL per 10 minutes. We allowed for a 10-minute period post injection for bolus diffusion before removing the injection needle. Postoperative care included closure of the cranial incision with sutures and veterinary tissue adhesive, and application of topical triple antibiotic ointment to the incision site. Animals were monitored while on a heating pad until they full recovery from the anesthetic.

Cannula Implantation The surgical protocol was the same as described above for viral injections. Fiber optic implants were fabricated using zirconia ferrules (Thorlabs) and from 100μm diameter fibre (0.22 numerical aperture (NA), Thorlabs). Fiber optic cannulas (length 5mm) were implanted at the CeA and the PAG and fixed to the skull using two bone screws (CMA anchor screws, #7431021) and dental cement. The following

18

1 coordinates were used for implantation: CeA, -1.24 mm from bregma, +/- 2.8 mm lateral

2 from midline and 4.25 mm ventral to skull and the PAG, -4.84 mm from bregma, +/- 0.5

3 mm lateral from midline and 2.7 mm ventral to skull. Mice were allowed to recover for 14

4 days before behavioral analysis. Animals in which cannulas placement missed the CeA

5 or vlPAG target were excluded from the study.

6 **Chemogenetic manipulation**

7 For chemogenetic control of CeA FosTRAPped neurons, cFos-Cre mice were injected

8 with Cre dependent control mCh, hM3Di or hM4Dq viruses. DREADD constructs used in

9 this study were validated previously in our lab for their functional expression in the PAG,

10 including their ability to increase (hM3Dq) or decrease (hM4Di) neuronal firing in slices

11 from animals expressing these viral constructs (Samineni et al., 2017a). Three weeks

12 later mice were injected with 4-OHT to express Cre dependent DREADDs, clozapine N-

13 oxide (CNO, BML-NS105 from Enzo life sciences) was injected 30 min before doing

14 behavioral experiments and data were collected between 30 min- and 2-hours post-

15 injection. All baselines for pruritic responses were recorded 3 weeks after the FosTRAP

16 and one week prior to the CNO administration. We used 5 mg/kg CNO as a dose of CNO

17 and showed no signs of behavioral changes in control vector-expressing animals.

18 **Optogenetic manipulations**

19 For all the behavioral experiments mice were acclimated to tethered fibers for 5 days

20 before initiation of the experiments. Mice were habituated to tethering with lightweight

21 patch cables (components: Doric lenses) that are connected to a laser (Shanghai laser,

22 475nm). To prevent impediment of movement from the tethered cables, we coupled patch

23 cables to an optical commutator (Doric Lenses). An arduino was programed and

24 connected to the laser to deliver 5, 10, 20 and 30 Hz (5-ms width, 10mW/mm^2)

25 photostimulation in FosCre mice.

26 **Activity-dependent FosTRAP labeling**

27 *4-hydroxytamoxifen preparation and delivery:* We dissolved 10 mg of 4-OHT (Sigma,

28 Cat# H6278-10MG) in 500ul ethanol (100%) (20mg/ml stock) first by vortexing and then

19

1   sonicating. ,We then add autoclaved corn oil (1:4) to dissolve 4-OHT (previously heated

2   to 45^0C) to 5mg/mL and sonicate until solution cloudiness clears. As a final step vacuum

3   centrifuge for 10 min to evaporate the alcohol from the final injection solution. Male

4   FosTRAP (FosCreER+/-, FosCreER+/-, Ai9+/-) mice were used. Mice were single housed

5   and gently handled for 7-10 days prior to the experiment to minimize the unwanted

6   labelling of neurons associated with stress of handling. On the experiment day mice were

7   given 4OHT 20mg/kg in their homecage environment. 60 Min post 4-OHT, we injected

8   either saline or chloroquine (200ug/50ul) subcutaneously in the nape of the neck to TRAP

9   neurons that are activated by pruritic stimuli. In FosCreER+/-, Ai9+/- mice, robust

10   tdTomato expression was seen 1 week post TRAPing. In the FosCreER+/- mice injected

11   with the optogenetic or chemogenetic constructs, robust labelling was seen 4 weeks post

12   TRAPing.

13   **Pruritic agent induced scratching behaviors**

14   As previously described by our group (O'Brien et al., 2013; Valtcheva et al., 2015), the

15   nape of the neck of mice was shaved one day prior to experiments. Mice were then placed

16   in clear plexiglass behavioral boxes for at least two hours for acclimation. For

17   chemogenetic manipulations, CNO was administered before placing the mice in the

18   plexiglass behavioral boxes and chloroquine (200μg/50μl, nape of the neck) induced

19   scratching behavior was performed 90 min after the CNO administration.

20   **Pain behavior assessment**

21   Mechanical sensitivity was measured by counting the number of withdrawal responses to

22   10 applications of von Frey filaments (North Coast Medical, Inc, Gilroy, CA; 0.02, 0.08,

23   0.32 and 1.28 g von Frey filaments) to both hindpaws as described (Samineni et al.,

24   2017c) . Each mouse was allowed at least 15 seconds between each application and at

25   least 5 minutes between each size filament. Animals were acclimated to individual boxes

26   on a plastic screen mesh for at least one hour before testing. The Hargreaves test was

27   performed to evaluate heat sensitivity thresholds as previously described (Samineni et

28   al., 2017a). Briefly, we measured latency of withdrawal to a radiant heat source (IITC Life

29   Science, Model 390). We applied the radiant heat source to both hindpaws and measured

1 the latency to evoke a withdrawal. Three replicates were acquired per hindpaw per mouse

2 and values for both paws were averaged.

3 **Open-Field test (OFT)**

4 Before testing, mice were habituated to the test room in their home cages for 2 h. Control

5 and mice injected with either hM3Dq, hM4Di or ChR2 in the CeA were then placed in the

6 open field during individual trials and allowed to freely explore after the experimenter

7 exited the room (behaviors were video recorded). Open field locomotor activity was

8 assessed in a square enclosure (55 x 55 cm) within a sound attenuated room for 30 min

9 (Shin et al., 2017). Total distance traveled and movements were video recorded and

10 analyzed using Ethovision XT (Noldus Information Technologies, Leesburg, VA).

11 **Elevated Zero maze (EZM)**

12 Anxiety was measured in low light conditions (~20 lux) using a modified zero maze

13 (Stoelting Co., Wood Dale, IL) placed 70 cm off of the ground and consisting of two closed

14 sections (wall height, 30 cm) and two open sections (wall height, 1.3 cm) on a circular

15 track (diameter of track, 60 cm)(Montana et al., 2011). On the experiment day mice were

16 habituated to testing room for 1 h before beginning of the behavioral session. For hM3Dq

17 and hM4Di injected mice 60 minutes after CNO injection, mice were placed individually

18 at the intersection of the closed/open area of the zero maze for a 600-s trial. For Chr2

19 and eYFP FosTRAP mice, mice were connected to the fiber optic and placed at the

20 intersection of the closed/open area of the zero maze for a 600-s trial. Mice received 20

21 Hz (5ms width) photostimulation for the duration of the EZM trial. Movement during the

22 trial was video recorded using digital camera (Floureon HD) mounted on the ceiling of the

23 room. Total distance traveled, number of entries into open sections, and time spent in the

24 open sections was scored were video recorded and analyzed using Ethovision XT

25 (Noldus Information Technologies, Leesburg, VA).

26 **Realtime place aversion testing (RPA)**

27 Place aversion was tested in a custom designed two compartment chamber (52.5 x 25.5

28 x 25.5 cm) with a layer of corn cob bedding (Shin et al., 2017). Each mouse was placed

1 in the neutral area of the chamber and given free access to roam across both chambers.

2 Activity was continuously recorded through a video camera for a period of 20 min. Entry

3 into light-paired chamber triggered constant photostimulation at either 5Hz, 10Hz, 20Hz

4 or 30Hz (473 nm, 5 ms pulse width, ~10 mW light power). Entry into the other chamber

5 terminated the photostimulation. Photostimulation was counterbalanced across mice.

6 "Time-in-chamber" and heat maps were generated for data analysis using Ethovision XT

7 software (Noldus, Leesburg, VA).

Conditioned place aversion (CPA)

9 CPA was performed using an unbiased, counterbalanced three-compartment

10 conditioning apparatus as described (Land et al., 2009). Each chamber had a unique

11 combination of visual, properties (one side had black and white vertical walls, whereas

12 the other side had black and white horizontally striped walls). On the pre-conditioning day

13 (day 1), mice were allowed free access to all three chambers for 20 min. Behavioral

14 activity in each compartment was monitored and recorded with a video camera and

15 analyzed using Ethovision 8.5 (Noldus) or ANY-Maze software. Mice were randomly

16 assigned to saline and chloroquine compartments and received a saline injection (50µl)

17 in the nape of the neck and on the mouse caudal back, in the morning and a chloroquine

18 injection (200µg/50µl) in the nape of the neck and on the mouse caudal back in the

19 afternoon, at least 4 h after the morning training on 3 consecutive days (Day 2, 3 & 4). To

20 enhance the association of chloroquine induced scratching behavior with the paired

21 chamber, we administered chloroquine and left the mice in their holding cage for 4 min,

22 then placed them in the paired chamber during the time of the peak scratching response

23 (20 min in the chamber). To assess for place aversion, the mice were then allowed free

24 access to all three compartments on day 5 for 30 minutes (Tzschentke, 2007). Scores

25 were calculated by subtracting the time spent in the chloroquine-paired compartment,

26 post-test minus the pre-test. To test the effect of DREADD hM4Di activation on

27 chloroquine-induced place aversion, mice injected with AAV5-DIO-hM4Di–mCherry and

28 AAV5-DIO-mCherry were allowed free access to all three chambers for 30 min on the pre-

29 conditioning day (day 1). On day 2, 3 & 4, both cohorts received a saline injection (50µl)

30 in the nape of the neck and on the mouse caudal back, and this chamber was paired with

22

1 systemic saline injection 1 h before they were placed in the compartment in the morning

2 and a chloroquine injection (200μg/50μl) in the nape of the neck and on the caudal back

3 and this chamber was paired with systemic CNO injection 1 h before they were placed in

4 the compartment in the afternoon. To test the effect of DREADD hM4Di activation on

5 chloroquine-induced place aversion, the mice were allowed free access to the three

6 compartments on day 5 for 30 minutes. Scores were calculated by subtracting the time

7 spent in the chloroquine-paired compartment, post-test minus the pre-test.

Operant conditioning

9 Mice are food deprived to reach 90% of their body weight and trained to nose poke for

10 sucrose pellets for 7 days during daily 60 min sessions in a modular test chamber (Med

11 Associates) on a fixed-ratio 1 (FR1) schedule of reinforcement as previously described

12 by (Seo et al., 2016; Shin et al., 2017). A correct nose poke response in the active hole

13 resulted in a sucrose pellet delivery where an incorrect nose poke within the inactive hole

14 resulted in no sucrose pellet. On the experiment day, mice were administered CNO

15 followed by a 60 min operant self-stimulation session. To determine if DREADD

16 manipulation of FosTRAPed CeA neurons has any effect on the fixed-ratio 1 (FR1)

17 schedule of reinforcement, mice were given free access to nose poke the ports, three

18 successive nose pokes (FR3) to the active portal rewarded the mouse a sucrose pellet

19 delivery where an incorrect nose poke within the inactive hole resulted in no sucrose

20 pellet. On the experiment day, mice were administered CNO followed by a 60 min operant

21 self-stimulation session, to determine if DREADD manipulation of FosTRAPed CeA

22 neurons has any effect on fixed-ratio 3 (FR3) schedule of reinforcement.

Feeding behavior

24 Mice were given free access to a novel empty cage prior to the experiment day. Mice

25 were food-deprived overnight prior to the experiment day (Cai et al., 2014). Mice were

26 reintroduced into the same empty cage they had access to the prior day but with food

27 pellets and allowed to feed freely for 20 min on the experiment day. At the end of the

28 session, weight of the food pellet and the food debris left on the cage floor was measured

29 to calculate the food intake. To determine whether FosTRAPed CeA neurons modulate

23

1 feeding behaviors, mice were injected with CNO 60 min before the feeding test. Feeding

2 tests were performed between 2 p.m. and 7 p.m.

3 **Fiber Photometry**

4 For *in vivo* calcium imaging of CeA GABAergic neurons, we injected the CeA of Vgat-Cre

5 mice with Cre-dependent GCaMP6s (AAV-DJ EF1a-DIO-GCaMP6s, 3 x 10^{13} particles/ml,

6 Stanford vector core). Fiber optic probes were unilaterally implanted above the right CeA

7 (-1.24 mm from bregma, +/- 2.84 mm lateral from midline and 4.4 mm ventral to skull).

8 After 4 weeks of viral expression, mice were handled and acclimated by tethering as will

9 occur during imaging sessions, for 7 days in the test behavioral chamber. On the test day,

10 mice were habituated with the tethered fiber optic patch cord (0.48NA, BFH48-400, Doric

11 lenses) in the test chamber (15 × 15cm) for 60 min and then injected with chloroquine

12 (200ug/50ul) in the nape of the neck and recordings were performed.

13 A fiber optic patch cord was used to connect to the fiber implant and deliver light

14 to excite and record the GCAMP signal using a custom-built fiber photometry rig, built

15 with some modifications to previously described specifications (Cui et al., 2013).

16 Fluorescence excitation was provided by two LEDs at 211 and 537 Hz to avoid picking

17 up room lighting (M405FP1, M470F1; LED driver: LEDD1B; Thorlabs). Light was

18 bandpass filtered (FMC1+(405/10) -(475/28)_(525/45)_FC), Doric lenses) and delivered

19 to the CeA to excite GCaMP6s. The emitted light was bandpass filtered

20 (FMC1+_(405/10)-(475/28)_(525/45)_FC), Doric lenses) and sent to a photoreceiver to

21 detect the signal (Newport, 2151). The signal from the photoreceiver was recorded using

22 a RZ5P real-time processor (TDT). Data were acquired at 10 kHz and then demodulated

23 at 211 and 537 Hz. The demodulated signal was then low-pass filtered (4 Hz) in a custom

24 MATLAB script. The extracted 405 nm signal was then scaled to fit the GCaMP signal for

25 the recording session. To isolate the movement-corrected GCaMP signal from channel,

26 we subtracted the signal at 405 nm from the 475 nm GCaMP signal. dF/F was obtained

27 by dividing the final signal with its mean value. Behavioral event timestamps associated

28 with chloroquine evoked scratching behavior were scored and aligned with GCaMP signal

29 in the MATLAB script to create pre- and peri-stimulus time bins. To obtain pre- and peri-

30 stimulus chloroquine evoked scratching events, if the scratching events happened close

1 to each other (in a 30 second window) they we combined and scored as one bout. Z-
2 score was obtained by subtracting the mean of the GCaMP signal from the bin value of
3 the GCaMP signal and dividing it with the standard deviation of the bin value of the
4 GCaMP signal.

5 **Acute slice electrophysiology**

6 To determine the functional effects of chemogenetic manipulations in the itch
7 FosTRAPped CeA neurons, we performed targeted whole-cell patch-clamp recordings in
8 acute coronal slices from cFos-Cre mice expressing either hM3Dq or hM4Di receptors as
9 previously described(Samineni et al., 2017a). Mice used for electrophysiology and
10 behavioral studies were between 8-16 weeks of age. Three weeks after viral injections,
11 we performed itchTRAP and waited 3 weeks for expression of hM3Dq or hM4Di in the
12 CeA. Coronal slices containing the CeA were prepared and CeA neurons were visualized
13 through a 40x objective using IR-DIC microscopy on an Olympus BX51 microscope, and
14 mCherry+ cells were identified using epifluorescent illumination with a green LED (530
15 nm; Thorlabs), coupled to the back-fluorescent port of the microscope. Whole cell
16 recordings of itch FosTRAPed CeA neurons expressing hM3Dq-mCherry and hM4Di-
17 mCherry were performed using a Heka EPC 10 amplifier (Heka) with Patchmaster
18 software (Heka). Following stable 5 min whole-cell recordings (baseline), the effects of
19 either hM3Dq or hM4Di receptor activation on cellular excitability was isolated by blocking
20 AMPA/KARs (10 µM NBQX, Abcam), NMDARs (50 µM D-APV, Abcam), GABAARs (100
21 µM picrotoxin, Abcam), and GABABRs (50 µM baclofen, Abcam), and aCSF solution
22 containing 10 µM CNO added to the antagonist cocktail above was bath applied to the
23 brain slice.

24 **Immunohistochemistry**

25 Adult mice were deeply anesthetized using a ketamine/xylazine cocktail and then
26 perfused with 20ml of phosphate-buffered saline (PBS) and 4% paraformaldehyde
27 (weight/volume) in PBS (PFA; 4 °C). *For Fos staining:* To determine the causal
28 contribution of the CeA neuron in itch processing, we gave chloroquine to the nape of the
29 neck and 90 min later mice were perfused. To verify whether itch TRAPped tdTomato+

1   CeA neurons are faithfully TRAPed to pruritic stimulus and rule out non-specific labeling,

2   one week after the TRAP, we gave a second chloroquine injection and 90 min later mice

3   were perfused. Brains were carefully removed, post fixed in 4% PFA overnight and later

4   cryoprotected by immersion in 30% sucrose for at least 48 hrs. Tissues were mounted in

5   OCT while allowing solidification of the mounting medium at -80 °C. Using a cryostat,

6   30μm tissue sections were collected and stored in PBS1x 0.4% sodium azide at 4 °C.

7   After washing the sections in PBS1x, we blocked using 5% normal goat serum and 0.2%

8   Triton-X PBS 1x for one hour at room temperature. Primary antibodies against mCherry

9   (Mouse, Clontech, 632543; 1/500), GFP (rabbit polyclonal anti-GFP, Aves A11122;

10 1/500) and cFos, (rabbit monoclonal anti-phospho-cFos, Cell Signaling Ser32 D82C12;

11 1:2000) were diluted in blocking solution and incubated overnight at 4 °C. After three 10-

12 minute washes in PBS1x, tissues were incubated for one hour at room temperature with

13 secondary antibodies (Life Technologies: Alexa Fluor488 donkey anti rabbit IgG (1/500);

14 Alexa Fluor 488 goat anti rabbit (1/500); Alexa Fluor 555 goat anti mouse (1/500) Alexa

15 Fluor 555 goat anti rabbit (1/500)) and Neurotrace (435/455nm, 1/500) at room

16 temperature. Three PBS1x washes followed before sections were mounted with

17 Vectashield (H-1400) hard mounting media and imaged after slides cured. Images were

18 obtained on a Nikon Eclipse 80i epifluorescence microscope.

19 **Tissue preparation for RNAseq and Fac Sorting**

20 Animals (8-10-week-old, 7-10 days post TRAP) were used for this experiment to ensure

21 robust Ai9 reporter expression, while assuring fully developed brains. RNA-seq of the

22 TRAPped neurons was performed using protocols modified from prior published work to

23 improve neuronal survival (Arttamangkul et al., 2006; Guez-Barber et al., 2012; Hempel

24 et al., 2007). Animals were anesthetized with ketamine cocktail, perfused with aCSF (124

25 mM NaCl, 24 mM NaHCO$_3$, 12.5 mM glucose, 2.5 mM KCl, 1.25 mM NaH$_2$PO$_4$, 2 mM

26 CaCl$_2$, 1 mM MgCl$_2$, 5mM HEPES, pH 7.4, 300-310 mOsm) and decapitated for brain

27 removal. The brains were allowed to rest in cold oxygenated (95% O$_2$/5% CO$_2$) aCSF and

28 then sliced coronally using a vibratome (Leica VT1000 S). Brain slices (400-μm thick

29 sections) were collected and kept in cold oxygenated aCSF. Tissues were micro-

30 dissected under a microscope (Leica S9i) using a reusable 0.5mm biopsy punch (WPI

1   504528). HBSS+H and Papain solution (45U, Worthington, Lakewood, NJ)) was

2   incubated for 5min at 37 degrees, followed by the addition of tissue punches for 10-15min.

3   Tissue punches were then transferred to ice, and mechanical trituration of tissue punches

4   was performed using ~600, 300 and 150 μm fire-polished Pasteur pipettes. The resulting

5   cell suspension was then centrifuged at 5k RPM for 5min to obtain a pellet, and cells were

6   re-suspended in fresh aCSF. This process happened twice to wash any remnants of

7   Papain. Cells were ultimately resuspended for FACS sorting into cold oxygenated aCSF

8   and kept on ice for the duration of the experiment.

9   Cell suspensions were kept cold throughout the FACS, and cells were sorted in aCSF. In

10 order to determine gating criteria for selecting cell bodies while excluding debris, we

11 performed FACS on fixed/permeabilized neurons stained with Neurotrace 435/455nm

12 (Nissl stain). Samples were treated with 2% PFA for 20min, pelleted down for 5min at 5k

13 RPM, and then resuspended in PBS1x 0.3% Triton X-100. This processed was done an

14 additional time to get rid of any remnant of PFA. Cells were then resuspended in aCSF

15 and incubated with Neurotrace 435/455 (ThermoFisher, #N211479) for FACS sorting. We

16 gated for events which had high levels of Neurotrace, and then mapped these events in

17 the scatter plot (forward scatter FSC vs. side scatter SSC). We were able to map events

18 which had high Neurotrace expression to a small subset of events, which represent the

19 population of cell bodies and not debris. In addition, this population was sensitive to PFA

20 fixation and labeling with the nuclear staining DAPI or 7-AAD, which is characteristic of

21 post-fixative dead cells. As for DAPI/7-AAD (dead) control samples, these were incubated

22 in 2% PFA for 20min, pelleted down for 5min at 5k RPM, and then resuspended in PBS1x

23 0.3% Triton X-100, this processed was done an additional time to get rid of any remnant

24 PFA. Cells were then resuspended in aCSF and incubated with DAPI (1:1000 dilution of

25 1mg/mL DAPI, Thermo Fisher, #62248 or 7-AAD 7-Aminoactinomycin D, A1310, Thermo

26 Fisher) for FACS sorting. We performed control experiments to set the appropriate gates

27 for florescence, Ai9 (tdtomato) expression. Negative control samples were obtained from

28 c57BL6/J animals, while positive controls were obtained from Vgat Ai9. FosCre x Ai9

29 brains were used for isolation of the neuronal population of interest. The CeA was

30 dissociated as previously described (Guez-Barber et al., 2012), and cells were sorted into

31 a 96-well plate. Up to a maximum of 50 cells were sorted into one well filled with 9uL of

27

1   Clontech lysis buffer (Single-cell lysis buffer 10x, #635013 Takara Bio) + 5% RNAse
2   inhibitor (40U/ul, Promega RNAsin inhibitor N2511). Samples were then transferred to a
3   tube for processing by our Genome Technology Access Center (GTAC) core facility. ds-
4   cDNA was prepared using the SMARTer Ultra Low RNA kit for Illumina Sequencing
5   (Takara-Clontech) per manufacturer's protocol using the lysis buffer as substrate for the
6   reaction. cDNA was fragmented using a Covaris E220 sonicator using peak incident
7   power 18, duty factor 20%, cycles/burst 50, time 120 seconds. cDNA was blunt ended,
8   had an A base added to the 3' ends, and then had Illumina sequencing adapters ligated
9   to the ends. Ligated fragments were then amplified for 15 cycles using primers
10 incorporating unique index tags. Fragments were sequenced on an Illumina HiSeq-3000
11 using single reads extending 50 bases.

12 **RNAseq**

13 RNA-seq reads were aligned to the Ensembl top-level assembly with STAR version
14 2.0.4b. Gene counts were derived from the number of uniquely aligned unambiguous
15 reads by Subread:featureCount version 1.4.5. Transcript counts were produced by
16 Sailfish version 0.6.3. Sequencing performance was assessed for total number of aligned
17 reads, total number of uniquely aligned reads, genes and transcripts detected, ribosomal
18 fraction known junction saturation and read distribution over known gene models with
19 RSeQC version 2.3.

20 All gene-level and transcript counts were then imported into the R/Bioconductor package
21 EdgeR and TMM normalization size factors were calculated to adjust for samples for
22 differences in library size. Ribosomal features as well as any feature not expressed in at
23 least the smallest condition size minus one sample were excluded from further analysis
24 and TMM size factors were recalculated to created effective TMM size factors. The TMM
25 size factors and the matrix of counts were then imported into R/Bioconductor package
26 Limma and weighted likelihoods based on the observed mean-variance relationship of
27 every gene/transcript and sample were then calculated for all samples with the voom with
28 quality weights function.   Generalized linear models were then created to test for
29 gene/transcript level differential expression. Differentially expressed genes and
30 transcripts were then filtered for p-values less than or equal to 0.001.

The biological interpretation of the genes found in the Limma results were then queried for global transcriptomic changes in known Gene Ontology (GO) and KEGG terms with the R/Bioconductor packages GAGE and Pathview. Briefly, GAGE measures for perturbations in GO or KEGG terms based on changes in the observed log 2-fold-changes for the genes within that term versus the background log 2-fold-changes observed across features not contained in the respective term as reported by Limma. For GO terms with an adjusted statistical significance of FDR <= 0.05, heatmaps were automatically generated for each respective term to show how genes co-vary or co-express across the term in relation to a given biological process or molecular function. In the case of KEGG curated signaling and metabolism pathways, Pathview was used to generate annotated pathway maps of any perturbed pathway with an unadjusted statistical significance of p-value <= 0.05.

To find the most critical genes, the raw counts were variance stabilized with the R/Bioconductor package DESeq2 and was then analyzed via weighted gene correlation network analysis with the R/Bioconductor package WGCNA. Briefly, all genes were correlated across each other by Pearson correlations and clustered by expression similarity into unsigned modules using a power threshold empirically determined from the data. An eigengene was then created for each de novo cluster and its expression profile was then correlated across all coefficients of the model matrix. Because these clusters of genes were created by expression profile rather than known functional similarity, the clustered modules were given the names of random colors where grey is the only module that has any pre-existing definition of containing genes that do not cluster well with others. The information for all clustered genes for each module were then combined with their respective statistical significance results from Limma to determine whether or not those features were also found to be significantly differentially expressed. Raw and analyzed data can be found at GEO: GSE130268.

Fluorescence in situ hybridization (FISH)

C57BL/6 J mice were injected with chloroquine on the nape of the neck. Thirty minutes post chloroquine administration, mice were rapidly decapitated, brains were dissected and flash frozen in −50 °C 2-methylbutane and stored at −80 °C for further

29

1   processing(Samineni et al., 2017b). Coronal sections of the brain corresponding to the

2   CeA, were cut at 15 µM at −20°C and thaw-mounted onto Super Frost Plus slides (Fisher).

3   Slides were stored at −80 °C until further processing. FISH was performed according to

4   the RNAScope® 2.0 Fluorescent Multiple Kit v2 User Manual for Fresh Frozen Tissue

5   (Advanced Cell Diagnostics, Inc.). Slides containing CeA sections were fixed in 4%

6   paraformaldehyde, dehydrated, and pretreated with protease IV solution for 30 min.

7   Sections were then incubated with target probes for mouse cFos (mm-Fos, catalog

8   number 316921, Advanced Cell Diagnostics), Ntsr2 (mm- Ntsr2, catalog number 452311,

9   Advanced Cell Diagnostics), GPR88 (mm- GPR88, catalog number 317451, Advanced

10   Cell Diagnostics), Penk (mm-Penk, catalog number 318761, Advanced Cell Diagnostics),

11   Gabarg1 (mm-Gabarg1, catalog number 501401, Advanced Cell Diagnostics), Oprm1

12   (mm-Oprm1, catalog number 315841, Advanced Cell Diagnostics), Chrm1 (mm-Chrm1,

13   catalog number 495291, Advanced Cell Diagnostics) . Following probe hybridization,

14   sections underwent a series of probe signal amplification steps (AMP1–4) followed by

15   incubation of fluorescent probes (Opal 470, Opal 570, Opal 670), designed to target the

16   specified channel associated with the probes. Slides were counterstained with DAPI and

17   coverslips were mounted with Vectashield Hard Set mounting medium (Vector

18   Laboratories). Images were obtained on a Leica TCS SPE confocal microscope (Leica),

19   and Application Suite Advanced Fluorescence (LAS AF) software was used for analyses.

20   To quantify number of cFos+ve cells, we counted DAPI-stained nuclei that coexpress

21   minimum of five cFos puncta as an cFos+ve cell. We did not include any cFos puncta that

22   does not overlay on top of the DAPI-stained nuclei as part of our analysis.

23   **Statistics**

24   Throughout the study, researchers were blinded to all experimental conditions. Exclusion

25   criteria for our study consisted on a failure to localize expression in our experimental

26   models or off-site administration of virus or drug. At least 3 replicates measurements were

27   performed and averaged in all behavioral assays. The number of animals used is

28   indicated by the "N" in each experiment. When paired t Test was used for comparing

29   paired observations, we evaluated for normality using the D'Agostino and Pearson

30   omnibus normality test for all datasets. Therefore, only when normality could be assumed,

1 we used a parametric test to analyze out data. If normality could not be assumed, a

2 nonparametric test or a Wilcoxon matched pairs text was used to evaluate differences

3 between the means of our experimental groups. Two-way ANOVA was used for

4 comparing between different control and treatment groups. Bonferroni's *post hoc* tests

5 were used (when significant main effects were found) to compare effects of variables. A

6 value of p <0.05 was considered statistically significant for all statistical comparisons.

Acknowledgments

Author Contributions

20 V.K.S and R.W.G. designed the experiments; V.K.S., J.G.G., E.S.A, J.N.S, S.B.S.

21 performed anatomical analyses; V.K.S. and J.G.G. performed behavior; C.P wrote the

22 code for photometry analysis; G.E.G performed FACS for RNA-seq; E.T. Performed data

23 curation, analysis and methodology for RNA-seq; B.A.C. performed slice

24 electrophysiology; M.R.B. contributed reagents/resources; V.K.S., J.G.G., G.E.G.,

25 B.A.C., A.D.M, E.T., C.P, and R.W.G. analyzed the data; V.K.S., and R.W.G. wrote the

26 manuscript with comments from all the authors.

Code availability

28 Matlab code used in this study is available from the corresponding author upon request.

References:

Ahrens, S., Wu, M.V., Furlan, A., Hwang, G.R., Paik, R., Li, H.H., Penzo, M.A., Tollkuhn, J., and Li, B. (2018). A Central Extended Amygdala Circuit That Modulates Anxiety. Journal of Neuroscience *38*, 5567-5583.

Albisetti, G.W., Pagani, M., Platonova, E., Hosli, L., Johannssen, H.C., Fritschy, J.M., Wildner, H., and Zeilhofer, H.U. (2019). Dorsal Horn Gastrin-Releasing Peptide Expressing Neurons Transmit Spinal Itch But Not Pain Signals. J Neurosci *39*, 2238-2250.

Arttamangkul, S., Torrecilla, M., Kobayashi, K., Okano, H., and Williams, J.T. (2006). Separation of mu-opioid receptor desensitization and internalization: endogenous receptors in primary neuronal cultures. J Neurosci *26*, 4118-4125.

Avegno, E.M., Lobell, T.D., Itoga, C.A., Baynes, B.B., Whitaker, A.M., Weera, M.M., Edwards, S., Middleton, J.W., and Gilpin, N.W. (2018). Central Amygdala Circuits Mediate Hyperalgesia in Alcohol-Dependent Rats. J Neurosci *38*, 7761-7773.

Bautista, D.M., Wilson, S.R., and Hoon, M.A. (2014). Why we scratch an itch: the molecules, cells and circuits of itch. Nat Neurosci *17*, 175-182.

Botta, P., Demmou, L., Kasugai, Y., Markovic, M., Xu, C., Fadok, J.P., Lu, T., Poe, M.M., Xu, L., Cook, J.M.*, et al.* (2015). Regulating anxiety with extrasynaptic inhibition. Nat Neurosci *18*, 1493-1500.

Cai, H., Haubensak, W., Anthony, T.E., and Anderson, D.J. (2014). Central amygdala PKC-delta(+) neurons mediate the influence of multiple anorexigenic signals. Nat Neurosci *17*, 1240-1248.

Carrasquillo, Y., and Gereau, R.W.t. (2007). Activation of the extracellular signal-regulated kinase in the amygdala modulates pain perception. J Neurosci *27*, 1543-1551.

Carter, M.E., Soden, M.E., Zweifel, L.S., and Palmiter, R.D. (2013). Genetic identification of a neural circuit that suppresses appetite. Nature *503*, 111-114.

Chen, L., Wang, W., Tan, T., Han, H., and Dong, Z. (2016). GABA(A) Receptors in the Central Nucleus of the Amygdala Are Involved in Pain- and Itch-Related Responses. J Pain *17*, 181-189.

Ciocchi, S., Herry, C., Grenier, F., Wolff, S.B., Letzkus, J.J., Vlachos, I., Ehrlich, I., Sprengel, R., Deisseroth, K., Stadler, M.B.*, et al.* (2010). Encoding of conditioned fear in central amygdala inhibitory circuits. Nature *468*, 277-282.

Crock, L.W., Kolber, B.J., Morgan, C.D., Sadler, K.E., Vogt, S.K., Bruchas, M.R., and Gereau, R.W.t. (2012). Central amygdala metabotropic glutamate receptor 5 in the modulation of visceral pain. J Neurosci *32*, 14217-14226.

Cui, G., Jun, S.B., Jin, X., Pham, M.D., Vogel, S.S., Lovinger, D.M., and Costa, R.M. (2013). Concurrent activation of striatal direct and indirect pathways during action initiation. Nature *494*, 238-242.

Desbordes, G., Li, A., Loggia, M.L., Kim, J., Schalock, P.C., Lerner, E., Tran, T.N., Ring, J., Rosen, B.R., Kaptchuk, T.J.*, et al.* (2015). Evoked itch perception is associated with changes in functional brain connectivity. Neuroimage Clin *7*, 213-221.

Douglass, A.M., Kucukdereli, H., Ponserre, M., Markovic, M., Grundemann, J., Strobel, C., Morales, P.L.A., Conzelmann, K.K., Luthi, A., and Klein, R. (2017). Central amygdala circuits modulate food consumption through a positive-valence mechanism. Nature Neuroscience *20*, 1384-+.

Ehling, S., Butler, A., Thi, S., Ghashghaei, H.T., and Baumer, W. (2018). To scratch an itch: Establishing a mouse model to determine active brain areas involved in acute histaminergic itch. IBRO Rep *5*, 67-73.

Ehrlich, I., Humeau, Y., Grenier, F., Ciocchi, S., Herry, C., and Luthi, A. (2009). Amygdala inhibitory circuits and the control of fear memory. Neuron *62*, 757-771.

Fadok, J.P., Markovic, M., Tovote, P., and Luthi, A. (2018). New perspectives on central amygdala function. Curr Opin Neurobiol *49*, 141-147.

Gao, Z.R., Chen, W.Z., Liu, M.Z., Chen, X.J., Wan, L., Zhang, X.Y., Yuan, L., Lin, J.K., Wang, M., Zhou, L.*, et al.* (2019). Tac1-Expressing Neurons in the Periaqueductal Gray Facilitate the Itch-Scratching Cycle via Descending Regulation. Neuron *101*, 45-+.

Ginsburg, I.H. (1995). Psychological and psychophysiological aspects of psoriasis. Dermatol Clin *13*, 793-804.

Grundemann, J., and Luthi, A. (2015). Ensemble coding in amygdala circuits for associative learning. Curr Opin Neurobiol *35*, 200-206.

1   Guenthner, C.J., Miyamichi, K., Yang, H.H., Heller, H.C., and Luo, L. (2013). Permanent
2   genetic access to transiently active neurons via TRAP: targeted recombination in active
3   populations. Neuron *78*, 773-784.

4   Guez-Barber, D., Fanous, S., Harvey, B.K., Zhang, Y., Lehrmann, E., Becker, K.G.,
5   Picciotto, M.R., and Hope, B.T. (2012). FACS purification of immunolabeled cell types
6   from adult rat brain. J Neurosci Methods *203*, 10-18.

7   Han, L., and Dong, X. (2014). Itch mechanisms and circuits. Annu Rev Biophys *43*, 331-
8   355.

9   Han, W., Tellez, L.A., Rangel, M.J., Jr., Motta, S.C., Zhang, X., Perez, I.O., Canteras,
10   N.S., Shammah-Lagnado, S.J., van den Pol, A.N., and de Araujo, I.E. (2017). Integrated
11   Control of Predatory Hunting by the Central Nucleus of the Amygdala. Cell *168*, 311-
12   324 e318.

13   Hardaway, J.A., Halladay, L.R., Mazzone, C.M., Pati, D., Bloodgood, D.W., Kim, M.,
14   Jensen, J., DiBerto, J.F., Boyt, K.M., Shiddapur, A.*, et al.* (2019). Central Amygdala
15   Prepronociceptin-Expressing Neurons Mediate Palatable Food Consumption and
16   Reward. Neuron *102*, 1037-1052 e1037.

17   Haubensak, W., Kunwar, P.S., Cai, H., Ciocchi, S., Wall, N.R., Ponnusamy, R., Biag, J.,
18   Dong, H.W., Deisseroth, K., Callaway, E.M.*, et al.* (2010). Genetic dissection of an
19   amygdala microcircuit that gates conditioned fear. Nature *468*, 270-276.

20   Hempel, C.M., Sugino, K., and Nelson, S.B. (2007). A manual method for the
21   purification of fluorescently labeled neurons from the mammalian brain. Nat Protoc *2*,
22   2924-2929.

23   Ikoma, A., Steinhoff, M., Stander, S., Yosipovitch, G., and Schmelz, M. (2006). The
24   neurobiology of itch. Nat Rev Neurosci *7*, 535-547.

25   John, C.S., Sypek, E.I., Carlezon, W.A., Cohen, B.M., Ongur, D., and Bechtholt, A.J.
26   (2015). Blockade of the GLT-1 Transporter in the Central Nucleus of the Amygdala
27   Induces both Anxiety and Depressive-Like Symptoms. Neuropsychopharmacology *40*,
28   1700-1708.

29   Kalin, N.H., Shelton, S.E., and Davidson, R.J. (2004). The role of the central nucleus of
30   the amygdala in mediating fear and anxiety in the primate. J Neurosci *24*, 5506-5515.

1   Kim, J., Zhang, X., Muralidhar, S., LeBlanc, S.A., and Tonegawa, S. (2017). Basolateral

2   to Central Amygdala Neural Circuits for Appetitive Behaviors. Neuron *93*, 1464-1479

3   e1465.

4   LaMotte, R.H., Dong, X., and Ringkamp, M. (2014). Sensory neurons and circuits

5   mediating itch. Nat Rev Neurosci *15*, 19-31.

6   Land, B.B., Bruchas, M.R., Schattauer, S., Giardino, W.J., Aita, M., Messinger, D.,

7   Hnasko, T.S., Palmiter, R.D., and Chavkin, C. (2009). Activation of the kappa opioid

8   receptor in the dorsal raphe nucleus mediates the aversive effects of stress and

9   reinstates drug seeking. P Natl Acad Sci USA *106*, 19168-19173.

10 LeDoux, J. (2003). The emotional brain, fear, and the amygdala. Cell Mol Neurobiol *23*,

11 727-738.

12 LeDoux, J., and Daw, N.D. (2018). Surviving threats: neural circuit and computational

13 implications of a new taxonomy of defensive behaviour. Nature Reviews Neuroscience

14 *19*, 269-282.

15 Li, J.N., and Sheets, P.L. (2018). The central amygdala to periaqueductal gray pathway

16 comprises intrinsically distinct neurons differentially affected in a model of inflammatory

17 pain. J Physiol *596*, 6289-6305.

18 Li, M.J., Liu, L.Y., Chen, L., Cai, J., Wan, Y., and Xing, G.G. (2017). Chronic stress

19 exacerbates neuropathic pain via the integration of stress-affect-related information with

20 nociceptive information in the central nucleus of the amygdala. Pain *158*, 717-739.

21 Madisen, L., Zwingman, T.A., Sunkin, S.M., Oh, S.W., Zariwala, H.A., Gu, H., Ng, L.L.,

22 Palmiter, R.D., Hawrylycz, M.J., Jones, A.R.*, et al.* (2010). A robust and high-throughput

23 Cre reporting and characterization system for the whole mouse brain. Nat Neurosci *13*,

24 133-140.

25 Mochizuki, H., Hernandez, L., Yosipovitch, G., Sadato, N., and Kakigi, R. (2020). The

26 Amygdala Network for Processing Itch in Human Brains. Acta Derm Venereol *100*,

27 adv00345.

28 Mochizuki, H., Papoiu, A.D.P., Nattkemper, L.A., Lin, A.C., Kraft, R.A., Coghill, R.C.,

29 and Yosipovitch, G. (2015). Scratching Induces Overactivity in Motor-Related Regions

30 and Reward System in Chronic Itch Patients. J Invest Dermatol *135*, 2814-2823.

1 Mochizuki, H., Papoiu, A.D.P., and Yosipovitch, G. (2014). Brain Processing of Itch and

2 Scratching. In Itch: Mechanisms and Treatment, E. Carstens, and T. Akiyama, eds.

3 (Boca Raton (FL)).

4 Mochizuki, H., Tashiro, M., Kano, M., Sakurada, Y., Itoh, M., and Yanai, K. (2003).

5 Imaging of central itch modulation in the human brain using positron emission

6 tomography. Pain *105*, 339-346.

7 Montana, M.C., Conrardy, B.A., Cavallone, L.F., Kolber, B.J., Rao, L.K., Greco, S.C.,

8 and Gereau, R.W.t. (2011). Metabotropic glutamate receptor 5 antagonism with

9 fenobam: examination of analgesic tolerance and side effect profile in mice.

10 Anesthesiology *115*, 1239-1250.

11 Mu, D., Deng, J., Liu, K.F., Wu, Z.Y., Shi, Y.F., Guo, W.M., Mao, Q.Q., Liu, X.J., Li, H.,

12 and Sun, Y.G. (2017). A central neural circuit for itch sensation. Science *357*, 695-699.

13 Neugebauer, V., and Li, W. (2002). Processing of nociceptive mechanical and thermal

14 information in central amygdala neurons with knee-joint input. J Neurophysiol *87*, 103-

15 112.

16 O'Brien, D.E., Brenner, D.S., Gutmann, D.H., and Gereau, R.W.t. (2013). Assessment

17 of pain and itch behavior in a mouse model of neurofibromatosis type 1. J Pain *14*, 628-

18 637.

19 Papoiu, A.D., Coghill, R.C., Kraft, R.A., Wang, H., and Yosipovitch, G. (2012). A tale of

20 two itches. Common features and notable differences in brain activation evoked by

21 cowhage and histamine induced itch. Neuroimage *59*, 3611-3623.

22 Papoiu, A.D., Emerson, N.M., Patel, T.S., Kraft, R.A., Valdes-Rodriguez, R.,

23 Nattkemper, L.A., Coghill, R.C., and Yosipovitch, G. (2014). Voxel-based morphometry

24 and arterial spin labeling fMRI reveal neuropathic and neuroplastic features of brain

25 processing of itch in end-stage renal disease. J Neurophysiol *112*, 1729-1738.

26 Papoiu, A.D., Nattkemper, L.A., Sanders, K.M., Kraft, R.A., Chan, Y.H., Coghill, R.C.,

27 and Yosipovitch, G. (2013). Brain's reward circuits mediate itch relief. a functional MRI

28 study of active scratching. PLoS One *8*, e82389.

29 Ressler, K.J., and Mayberg, H.S. (2007). Targeting abnormal neural circuits in mood

30 and anxiety disorders: from the laboratory to the clinic. Nat Neurosci *10*, 1116-1124.

1 Robinson, M.J., Warlow, S.M., and Berridge, K.C. (2014). Optogenetic excitation of
2 central amygdala amplifies and narrows incentive motivation to pursue one reward
3 above another. J Neurosci *34*, 16567-16580.

4 Roozendaal, B., McEwen, B.S., and Chattarji, S. (2009). Stress, memory and the
5 amygdala. Nat Rev Neurosci *10*, 423-433.

6 Ross, S.E., Mardinly, A.R., McCord, A.E., Zurawski, J., Cohen, S., Jung, C., Hu, L.,
7 Mok, S.I., Shah, A., Savner, E.M.*, et al.* (2010). Loss of inhibitory interneurons in the
8 dorsal spinal cord and elevated itch in Bhlhb5 mutant mice. Neuron *65*, 886-898.

9 Samineni, V.K., Grajales-Reyes, J.G., Copits, B.A., O'Brien, D.E., Trigg, S.L., Gomez,
10 A.M., Bruchas, M.R., and Gereau, R.W. (2017a). Divergent Modulation of Nociception
11 by Glutamatergic and GABAergic Neuronal Subpopulations in the Periaqueductal Gray.
12 eNeuro *4*.

13 Samineni, V.K., Grajales-Reyes, J.G., Copits, B.A., O'Brien, D.E., Trigg, S.L., Gomez,
14 A.M., Bruchas, M.R., and Gereau, R.W.t. (2017b). Divergent Modulation of Nociception
15 by Glutamatergic and GABAergic Neuronal Subpopulations in the Periaqueductal Gray.
16 eNeuro *4*.

17 Samineni, V.K., Grajales-Reyes, J.G., Sundaram, S.S., Yoo, J.J., and Gereau, R.W.t.
18 (2019). Cell type-specific modulation of sensory and affective components of itch in the
19 periaqueductal gray. Nat Commun *10*, 4356.

20 Samineni, V.K., Mickle, A.D., Yoon, J., Grajales-Reyes, J.G., Pullen, M.Y., Crawford,
21 K.E., Noh, K.N., Gereau, G.B., Vogt, S.K., Lai, H.H.*, et al.* (2017c). Optogenetic
22 silencing of nociceptive primary afferents reduces evoked and ongoing bladder pain. Sci
23 Rep-Uk *7*.

24 Seo, D.O., Funderburk, S.C., Bhatti, D.L., Motard, L.E., Newbold, D., Girven, K.S.,
25 McCall, J.G., Krashes, M., Sparta, D.R., and Bruchas, M.R. (2016). A GABAergic
26 Projection from the Centromedial Nuclei of the Amygdala to Ventromedial Prefrontal
27 Cortex Modulates Reward Behavior. J Neurosci *36*, 10831-10842.

28 Shackman, A.J., and Fox, A.S. (2016). Contributions of the Central Extended Amygdala
29 to Fear and Anxiety. J Neurosci *36*, 8050-8063.

Shin, G., Gomez, A.M., Al-Hasani, R., Jeong, Y.R., Kim, J., Xie, Z.Q., Banks, A., Lee, S.M., Han, S.Y., Yoo, C.J*., et al.* (2017). Flexible Near-Field Wireless Optoelectronics as Subdermal Implants for Broad Applications in Optogenetics. Neuron *93*, 509-+.

Snow, M.B., Fraigne, J.J., Thibault-Messier, G., Chuen, V.L., Thomasian, A., Horner, R.L., and Peever, J. (2017). GABA Cells in the Central Nucleus of the Amygdala Promote Cataplexy. J Neurosci *37*, 4007-4022.

Steinberg, E.E., Gore, F., Heifets, B.D., Taylor, M.D., Norville, Z.C., Beier, K.T., Foldy, C., Lerner, T.N., Luo, L., Deisseroth, K*., et al.* (2020). Amygdala-Midbrain Connections Modulate Appetitive and Aversive Learning. Neuron *106*, 1026-1043 e1029.

Sun, Y.G., Zhao, Z.Q., Meng, X.L., Yin, J., Liu, X.Y., and Chen, Z.F. (2009). Cellular basis of itch sensation. Science *325*, 1531-1534.

Swanson, L.W., and Petrovich, G.D. (1998). What is the amygdala? Trends Neurosci *21*, 323-331.

Tovote, P., Esposito, M.S., Botta, P., Chaudun, F., Fadok, J.P., Markovic, M., Wolff, S.B., Ramakrishnan, C., Fenno, L., Deisseroth, K*., et al.* (2016). Midbrain circuits for defensive behaviour. Nature *534*, 206-212.

Tye, K.M., Prakash, R., Kim, S.Y., Fenno, L.E., Grosenick, L., Zarabi, H., Thompson, K.R., Gradinaru, V., Ramakrishnan, C., and Deisseroth, K. (2011). Amygdala circuitry mediating reversible and bidirectional control of anxiety. Nature *471*, 358-362.

Tzschentke, T.M. (2007). Measuring reward with the conditioned place preference (CPP) paradigm: update of the last decade. Addict Biol *12*, 227-462.

Valtcheva, M.V., Samineni, V.K., Golden, J.P., Gereau, R.W.t., and Davidson, S. (2015). Enhanced nonpeptidergic intraepidermal fiber density and an expanded subset of chloroquine-responsive trigeminal neurons in a mouse model of dry skin itch. J Pain *16*, 346-356.

Vierow, V., Forster, C., Vogelgsang, R., Dorfler, A., and Handwerker, H.O. (2015). Cerebral Networks Linked to Itch-related Sensations Induced by Histamine and Capsaicin. Acta Derm Venereol *95*, 645-652.

Warlow, S.M., Naffziger, E.E., and Berridge, K.C. (2020). The central amygdala recruits mesocorticolimbic circuitry for pursuit of reward or pain. Nat Commun *11*, 2716.

1 Weera, M.M., Schreiber, A.L., Avegno, E.M., and Gilpin, N.W. (2020). The role of
2 central amygdala corticotropin-releasing factor in predator odor stress-induced
3 avoidance behavior and escalated alcohol drinking in rats. Neuropharmacology *166*,
4 107979.
5 Yin, W., Mei, L., Sun, T., Wang, Y., Li, J., Chen, C., Farzinpour, Z., Mao, Y., Tao, W., Li,
6 J.*, et al.* (2020). A Central Amygdala-Ventrolateral Periaqueductal Gray Matter Pathway
7 for Pain in a Mouse Model of Depression-like Behavior. Anesthesiology *132*, 1175-
8 1196.
9 Zirlinger, M., and Anderson, D. (2003). Molecular dissection of the amygdala and its
10 relevance to autism. Genes Brain Behav *2*, 282-294.
11 Zirlinger, M., Kreiman, G., and Anderson, D.J. (2001). Amygdala-enriched genes
12 identified by microarray technology are restricted to specific amygdaloid subnuclei. Proc
13 Natl Acad Sci U S A *98*, 5270-5275.

14

15

16

17

18

19

20

21

22